INL/MIS-23-75206-Revision-0

Multi-scale modeling of the evolution of structure and properties in materials for nuclear energy applications

November 2023

Larry Kenneth Aagesen Jr

Changing the World's Energy Future

INL is a U.S. Department of Energy National Laboratory operated by Battelle Energy Alliance, LLC

INL/MIS-23-75206-Revision-0

Multi-scale modeling of the evolution of structure and properties in materials for nuclear energy applications

Larry Kenneth Aagesen Jr

November 2023

Idaho National Laboratory
Idaho Falls, Idaho 83415

http://www.inl.gov

Prepared for the
U.S. Department of Energy
Under DOE Idaho Operations Office
Contract DE-AC07-05ID14517

Multi-scale modeling of the evolution of structure and properties in materials for nuclear energy applications

Larry Aagesen
Idaho National Laboratory

Collaborators:
Sudipta Biswas, Kyle Gamble, Jacob Hirschhorn, Chao Jiang, Steve Novascone, Stephanie Pitts, Cheng Sun
Idaho National Laboratory

Benjamin Beeler, Wen Jiang
North Carolina State University

Yinbin Miao
Argonne National Laboratory

David Andersson, Michael Cooper, Christopher Matthews
Los Alamos National Laboratory

Edwin Garcia
Purdue University

Nuclear energy is an important part of an overall strategy to reduce carbon emissions

Utilities recently identify the need to add 100 gigawatts of nuclear power by 2050, more than doubling current capacity.

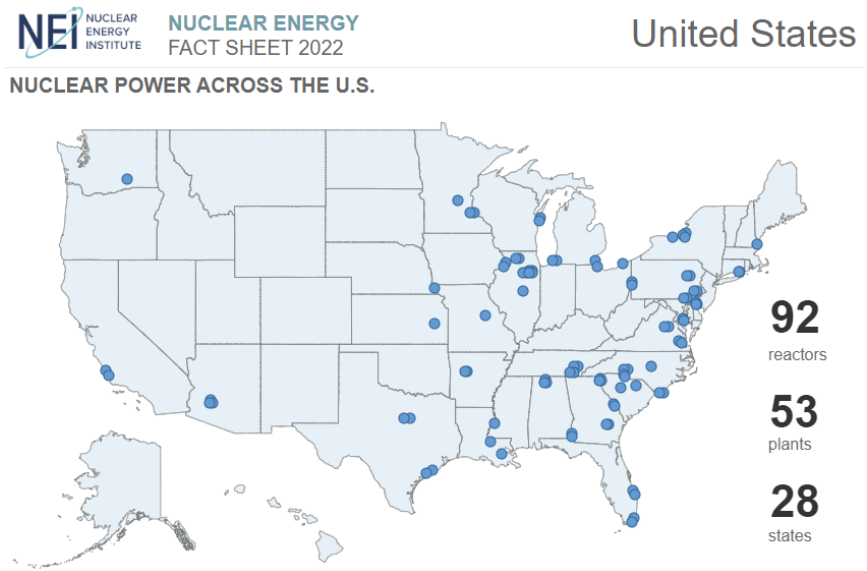

Today, 92 reactors provide nearly 20% of the electricity produced for our power grid and more than half of our carbon-free electricity – more than solar, wind, hydro, and geothermal combined.

- Utilities are prepared to invest in nuclear energy because it is a proven non-carbon-emitting solution
- Emissions avoided by adding 100 gigawatts of nuclear power is equivalent to taking more than 100 million cars off the road.
- New reactor designs are simpler, more versatile, and more economical at scale
- Utilities are evaluating reusing retired coal plant sites to leverage existing infrastructure and workforce

Idaho National Laboratory: Creating a secure and resilient clean energy future

INL mission: *Discover, demonstrate, and secure innovative nuclear energy solutions, clean energy options, and critical infrastructure.*

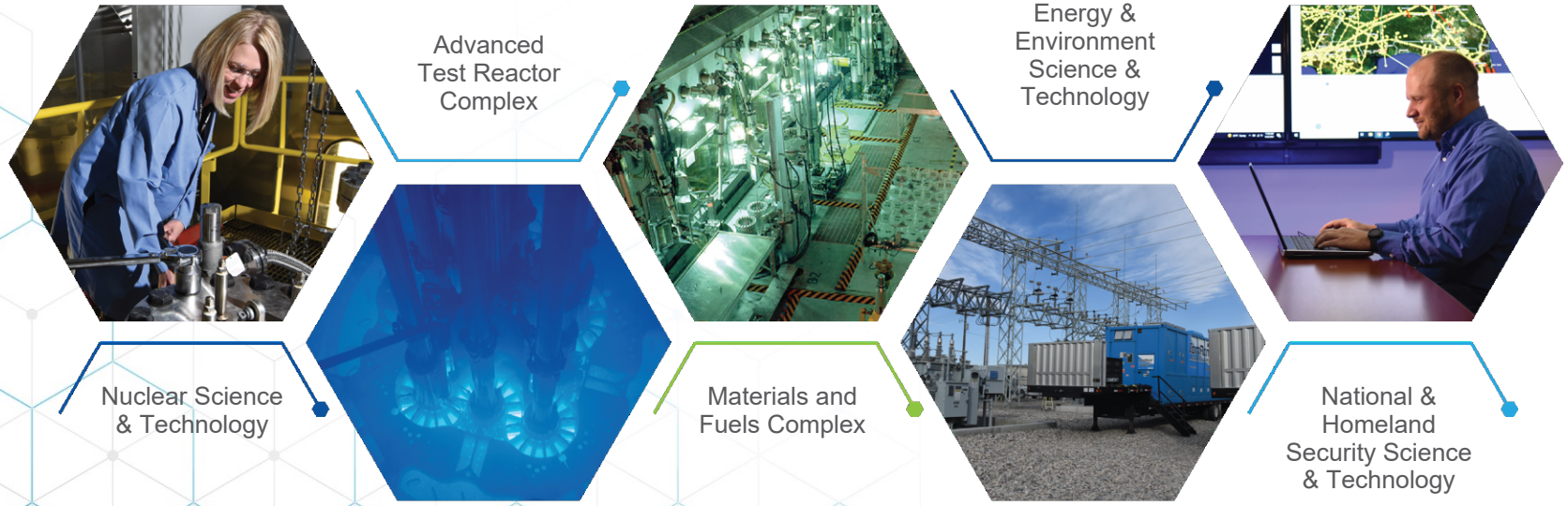

Mission-driven funding portfolio is growing and evolving

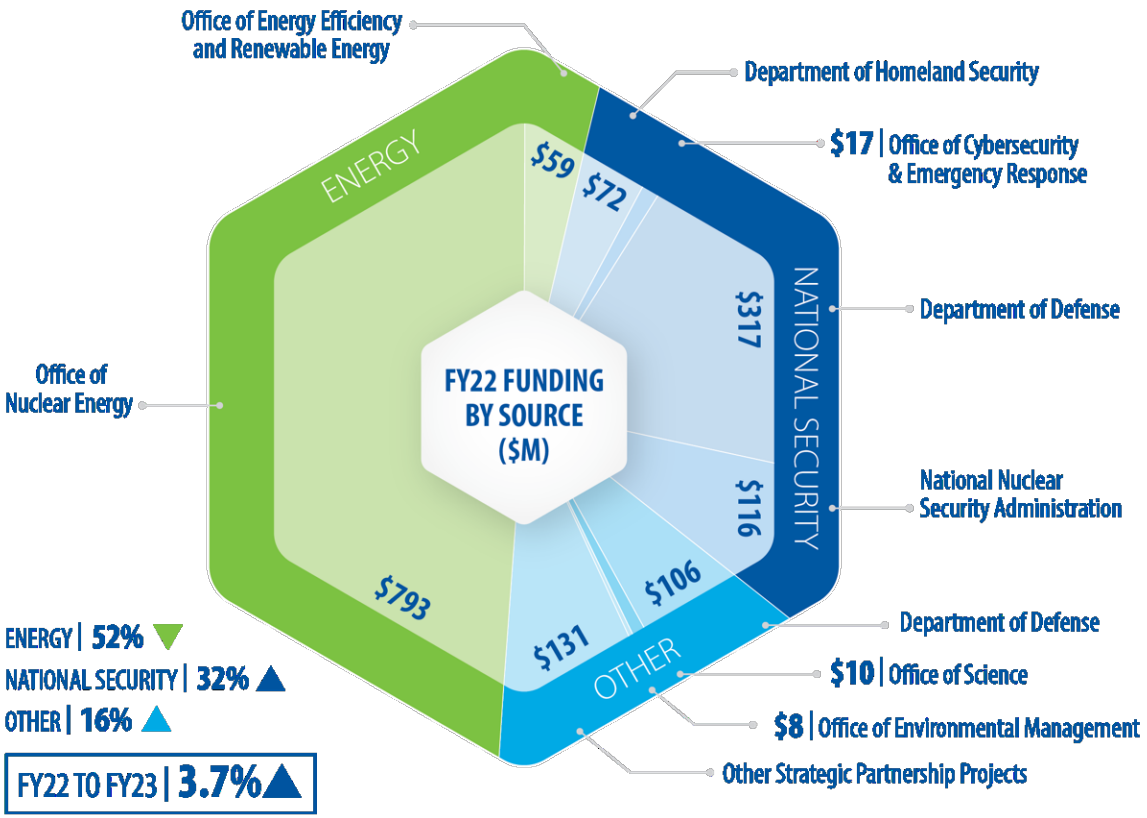

5th Largest DOE Laboratory

FY22 OPERATING COST

DOE/NNSA Costs: $1,092M
SPP (Non-DOE/Non-DHS): $445M
CRADA: $4M
DHS Costs: $89M
Total: $1,630M

FY22 HUMAN CAPITAL

5,594	full-time equivalent employees
40	joint appointments
102	postdoctoral researchers
511	interns
25	graduate fellows
36	visiting scientists
1,852	facility users

Sustaining the existing commercial reactor fleet and expanding deployment of future reactors

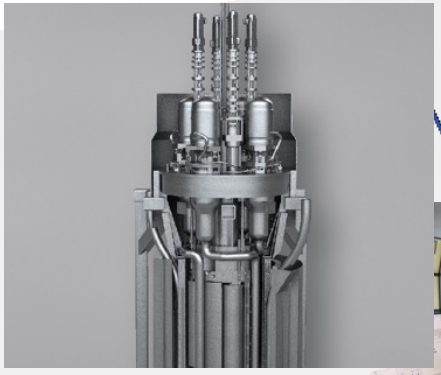

Regulatory and safety research

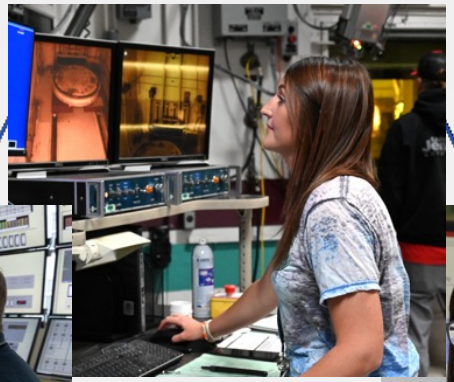

Advanced modeling and simulation

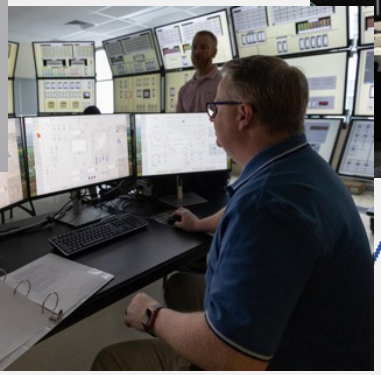

Advanced reactor technologies

Fuel cycle and separations

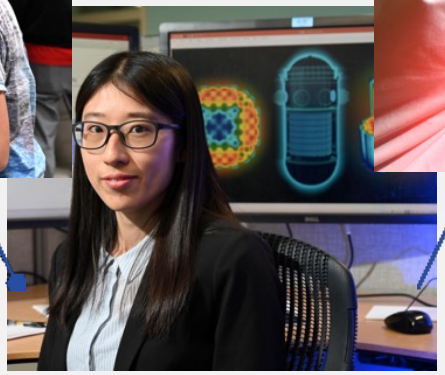

Nuclear fuels and materials

NRIC National Reactor Innovation Center

GAIN Gateway for Accelerated Innovation in Nuclear

IDAHO NATIONAL LABORATORY

Accelerating advanced reactor demonstration & deployment

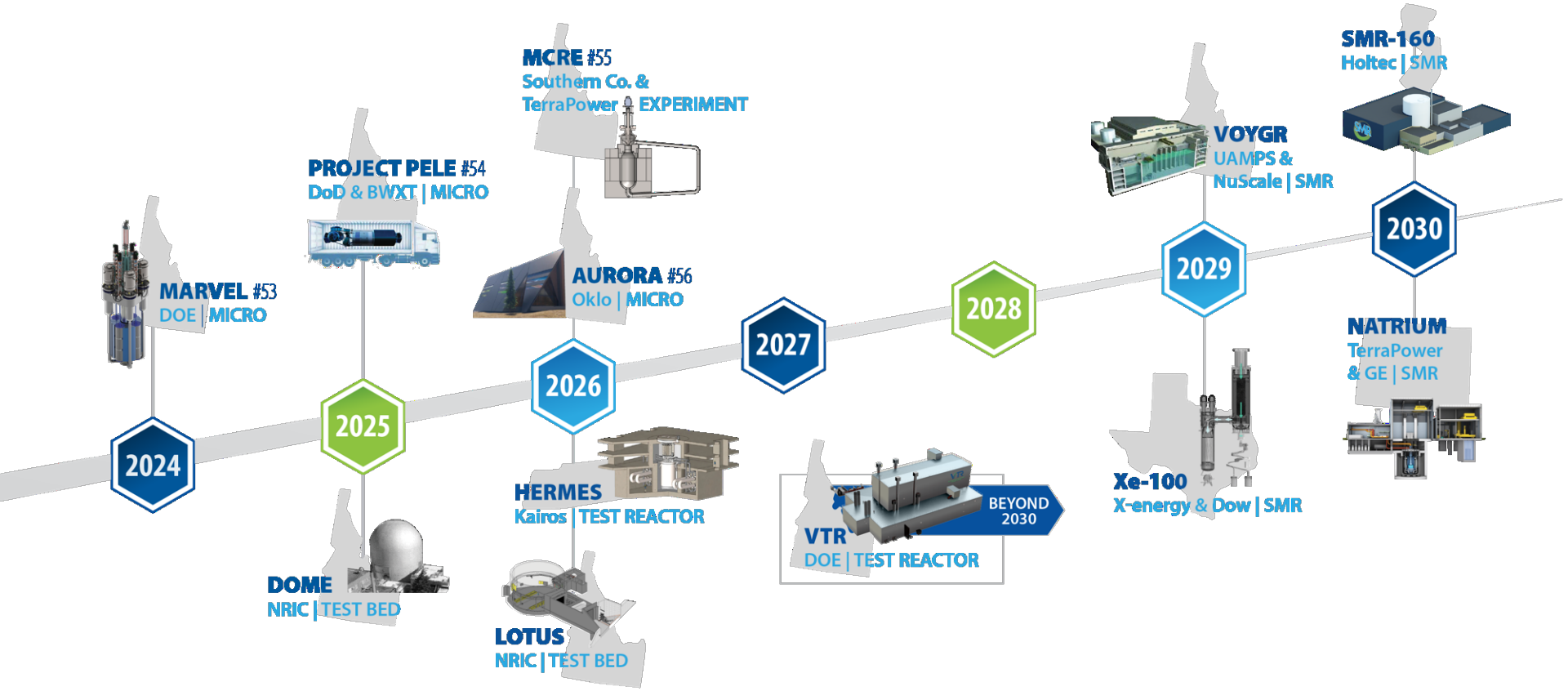

INL-University of Michigan Collaboration

- Memorandum of Understanding to enhance research collaboration
  - Signed early 2023, formal kickoff May 1-2 in Ann Arbor
- Selected topics of mutual interest: nuclear fuels and materials, materials science, advanced materials and manufacturing, multiphysics/reactor physics and design, integrated energy systems, mechanical engineering, cybersecurity of embedded systems, nuclear nonproliferation, and community engagement and environmental justice
- Concrete ways to work together:
  - Joint proposals (NEUP/IRP, ERFC)
  - Exchange/Training visits
  - Senior Design Project mentoring
  - Undergrad/grad internships
  - Co-recruiting graduate students
  - Joint appointments for faculty/staff

MEMORANDUM OF UNDERSTANDING

between

Battelle Energy Alliance, LLC (BEA)

AND

University of Michigan

on

STRATEGIC UNDERSTANDING FOR PREMIER EDUCATION & RESEARCH (SUPER)

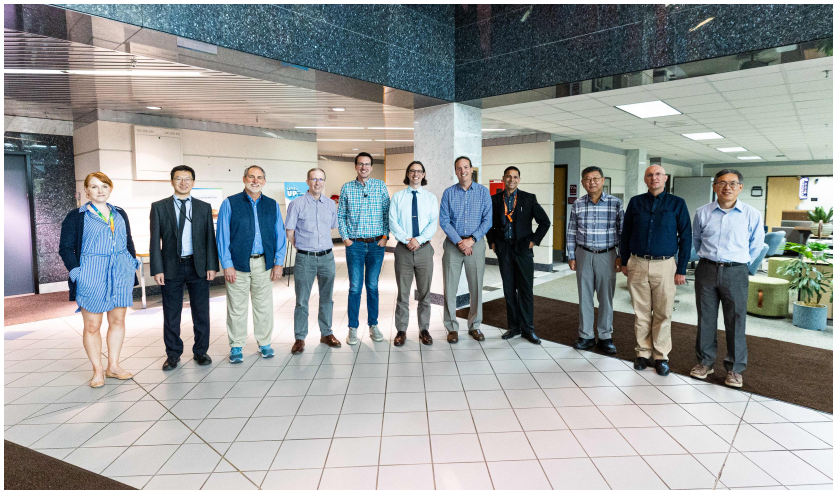

UM NERS Faculty Visit to INL
July 2023

MOOSE: Multi-physics Object-Oriented Simulation Environment

General purpose, open-source framework for solving partial differential equations

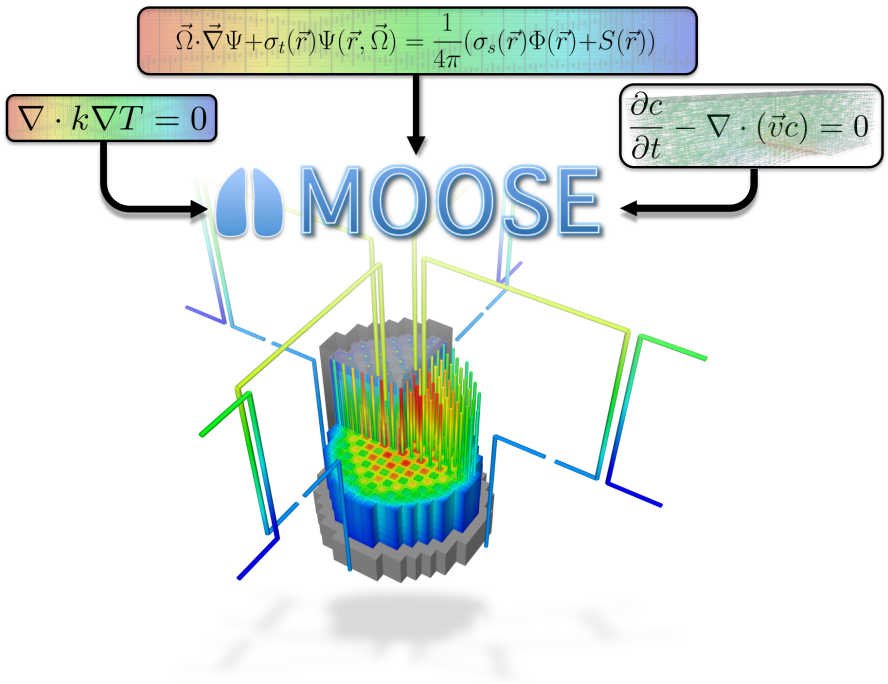

Capabilities:

- Continuous and Discontinuous Galerkin Finite Element Method
- Finite Volume
- Supports fully coupled or segregated systems, fully implicit and explicit time integration
- Automatic differentiation (AD)
- Unstructured mesh with FEM shapes
- Higher order geometry
- Mesh adaptivity (refinement and coarsening)
- Massively parallel (MPI and threads)
- User code agnostic of dimension, parallelism, shape functions, etc.

MOOSE Framework and Application Structure

Apps included with MOOSE

- Mechanics
- Phase-field
- Heat conduction
- Chemical reactions
- Navier-Stokes
- Electromagnetics

Open-source Apps

MALAMUTE

License-required Apps

MARMOT

BISON

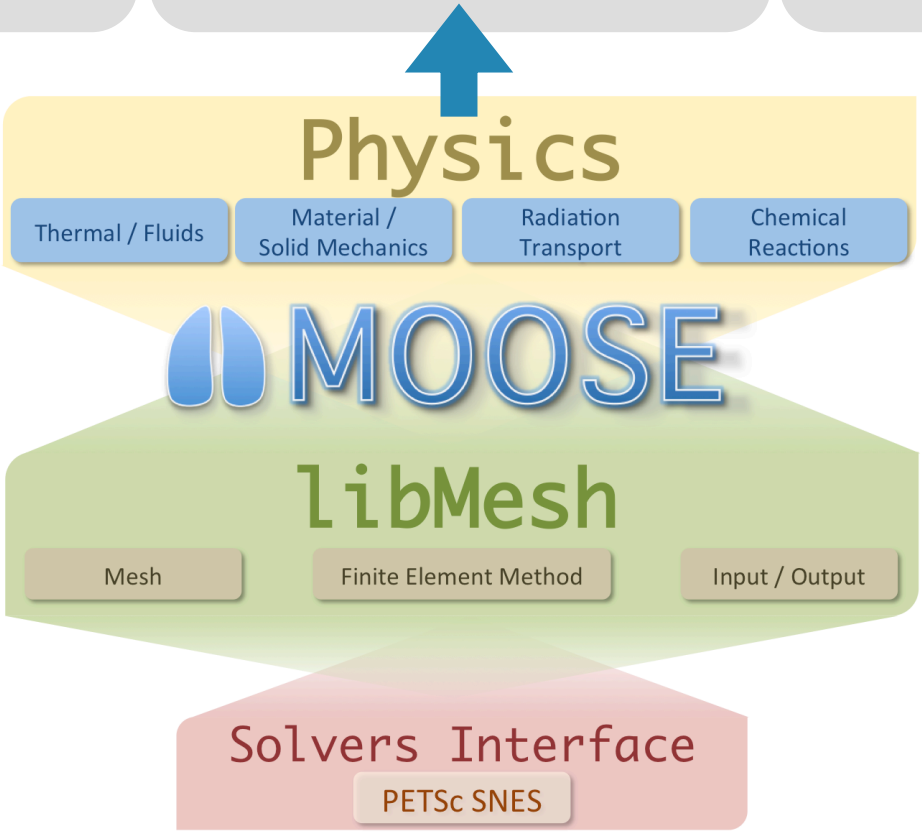

Multiscale nuclear fuel performance simulation

- BISON: MOOSE-Based Nuclear fuel performance code
- Inform BISON with atomistic and mesoscale simulations
  - Marmot: MOOSE-based phase-field simulation code

NEAMS
NUCLEAR ENERGY ADVANCED MODELING & SIMULATION PROGRAM

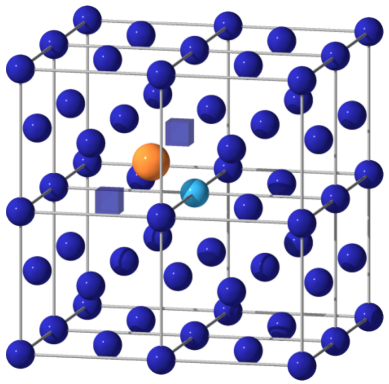

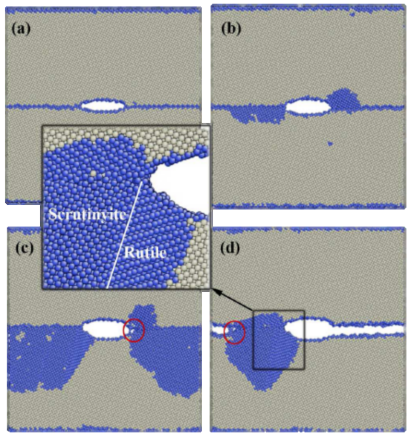

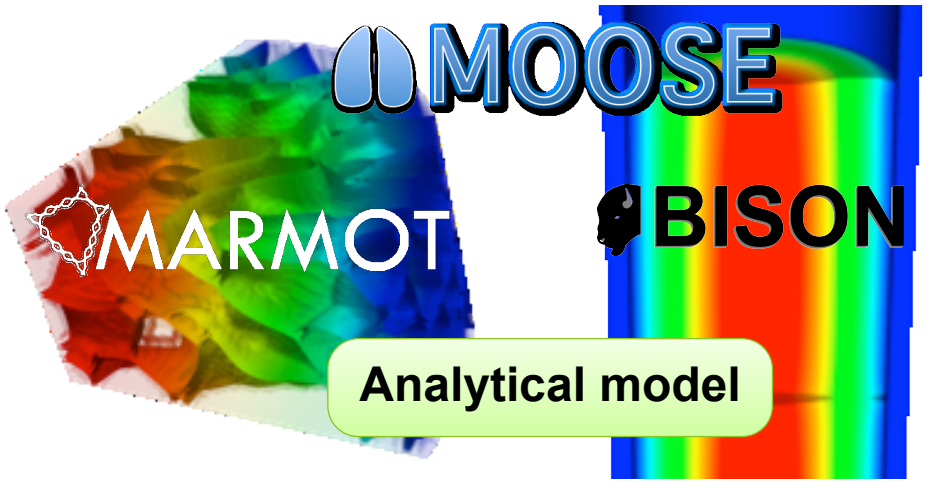

nanometers
First Principles
- Identify critical bulk mechanisms
- Determine bulk properties

100's of nanometers
Molecular Dynamics
- Identify interfacial mechanisms
- Determine interfacial properties

microns
Mesoscale
- Predict microstructure evolution
- Determine impact on properties

millimeters and up
Engineering Scale
- Use analytical theory
- Predict fuel performance

U_3Si_2 is being considered as a potential accident-tolerant fuel

- Compared with UO_2:
  - Lower melting temperature
  - But higher thermal conductivity may give higher margin to melting temperature
- U_3Si_2 swelling/fission gas release behavior less well characterized
  - Evidence from higher-temperature irradiation suggests pellet-form fuel would remain crystalline, have similar microstructure as UO_2 fuel
- BISON model recently developed based on these assumptions

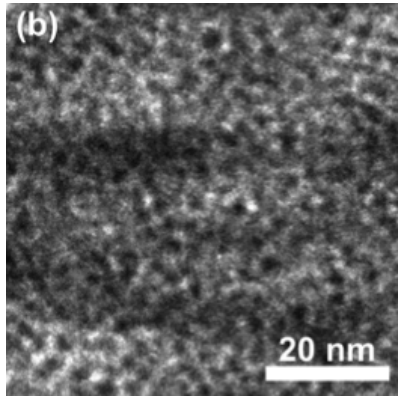

U_3Si_2 implanted with Xe at 873 K (Miao et al., J. Nuclear Mater., 503, 314-322 (2018).

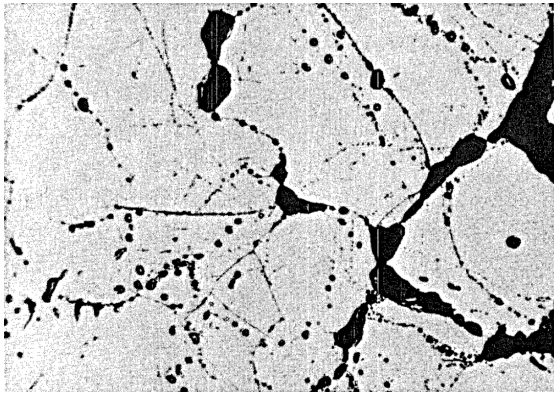

U_3Si_2 irradiated at ~950 K and ~6 GWd/tU (Shimizu, NAA-SR-1062, 1965).

Barani et al., J. Nuclear Mater., 522, 97-110 (2019).

Lower length scale calculations to reduce uncertainty in BISON

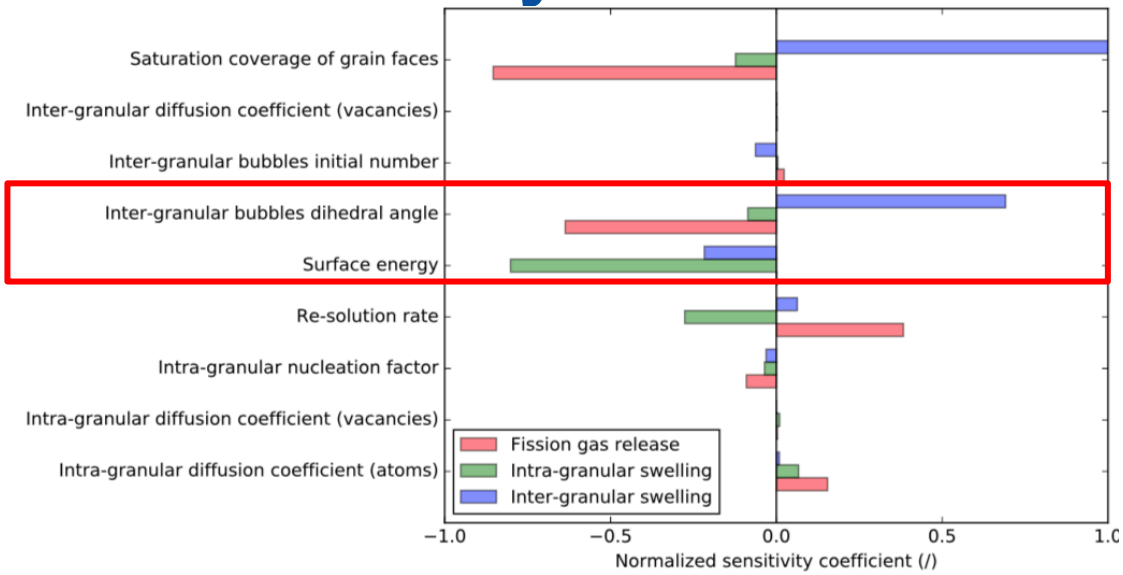

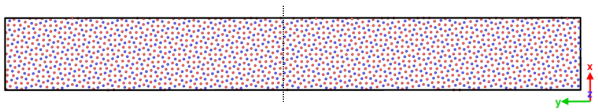

Configuration for MD Calculation of GB Energy

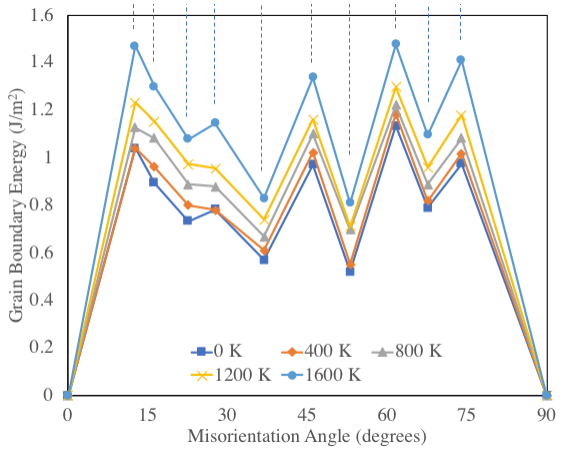

- Sensitivity analysis of BISON U_3Si_2 swelling and gas release predictions showed strong dependence on inter-granular bubble dihedral angle and surface energy
  - Measured values also not available
- Surface energy and grain boundary energies were determined for U_3Si_2 using molecular dynamics (MD) calculations
  - Dihedral angle (θ) calculated from surface energy and grain boundary energy; input to BISON
  - Data also used to parameterize Marmot model

Barani et al., J. Nuclear Mater., 522, 97-110 (2019).
Beeler, Baskes, Andersson, Cooper, Y. Zhang, J. Nucl. Mater., 514, 290-298 (2019).

Lower length scale calculations to reduce uncertainty in BISON

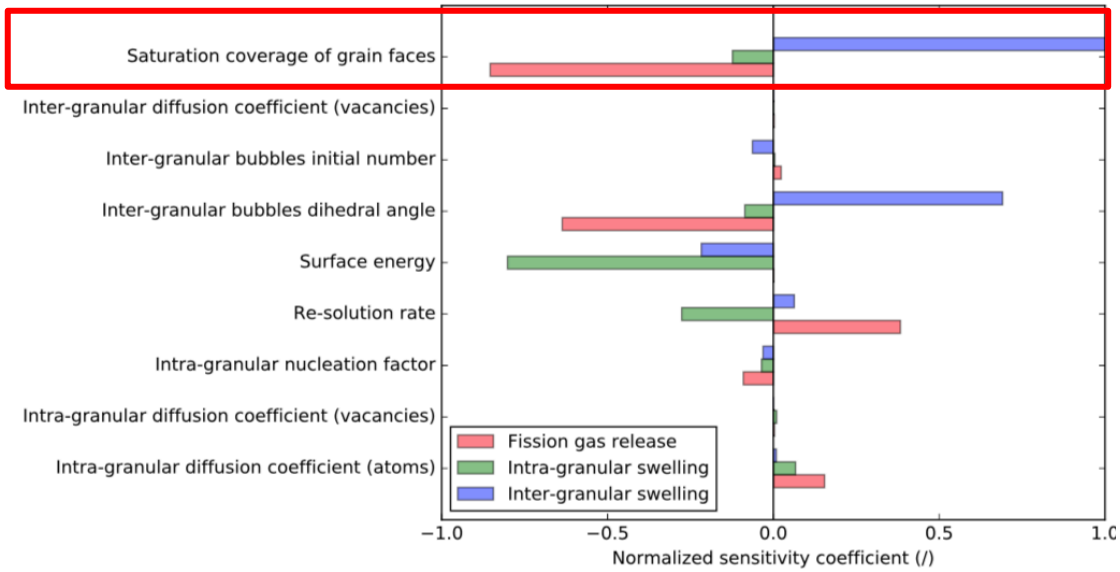

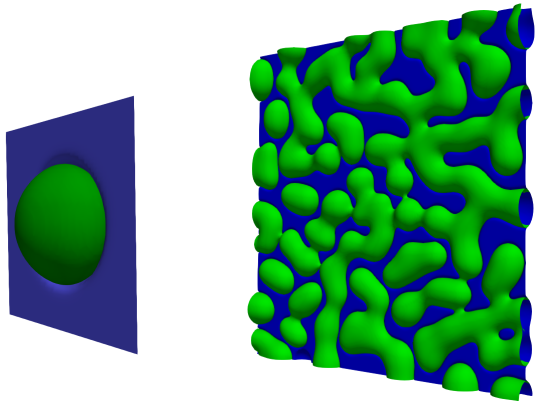

MARMOT

- Sensitivity analysis also showed strong dependence on saturation coverage of grain faces ($F_{c,sat}$)
  - No measured value available for U_3Si_2 , previous work used theoretical estimate of $F_{c,sat} = 0.78$
- Phase-field simulations[1] showed progress of grain boundary venting was strongly dependent on intergranular bubble areal density and dihedral angle
  - New phase-field simulations used to determine $F_{c,sat}$ using U_3Si_2 parameters

[1]Millett, Tonks, Biner, L. Zhang, Chockalingham, Y. Zhang, *J. Nucl. Mater.*, 425, 130-135 (2012).

Phase-field model: Essential physics

- Represent bubble phase and multiple grains of U_3Si_2
- Track vacancies and fission product species (Xe only)
  - Source terms for production
- Set surface energy and grain boundary energy
  - Controls dihedral angle θ
  - Remove bulk energy contribution to interfacial energy

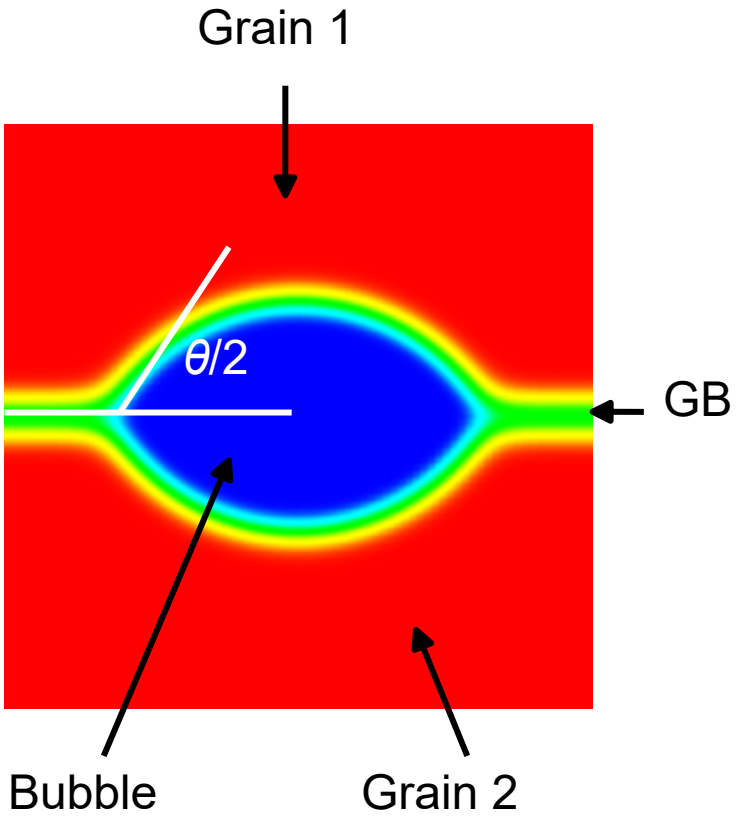

Phase-field model: Grand-potential functional

$$\Omega = \int_V \left(m \left[\sum_{\alpha} \sum_{i=1}^{p_\alpha} \left(\frac{\eta_{\alpha i}^4}{4} - \frac{\eta_{\alpha i}^2}{2} \right) + \sum_{\alpha} \sum_{i=1}^{p_\alpha} \left(\sum_{\beta} \sum_{j=1, \alpha i \neq \beta j}^{p_\beta} \frac{\gamma_{\alpha i \beta j}}{2} \eta_{\alpha i}^2 \eta_{\beta j}^2 \right) + \frac{1}{4} \right] + \frac{\kappa}{2} \sum_{\alpha} \sum_{i=1}^{p_\alpha} |\nabla \eta_{\alpha i}|^2 + \sum_{\alpha} h_\alpha \omega_\alpha \right) dV$$

- Multi-phase, multi-order parameter extension to grand-potential model
- Advantages:
  - Bulk free energy contribution is removed from interfacial energy
  - Allows interfacial thickness and energy to be set independently, enabling coarser mesh, improved computational performance
  - Similar to KKS in this respect, but do not need separate phase concentration variables, so performance is improved
  - Prevents spurious formation of additional phases at two-phase interfaces

M. Plapp
L.K. Aagesen, Y. Gao, D. Schwen, K. Ahmed, *Phys. Rev. E*, 98, 023309 (2018).
L.K. Aagesen, D. Schwen, M.R. Tonks, Y. Zhang, *Comp. Mat. Sci.*, 161, 35-45 (2019).

Phase-field model evolution equations

- Order parameters: Allen-Cahn
- Densities: Change to chemical potential for each species

Gas:

$$\frac{\partial \mu_g}{\partial t} = \frac{1}{\chi_g}\left[\nabla \cdot (D_g \chi_g \nabla \mu_g) + s_g - \sum_{\alpha}\sum_{i=1}^{p_\alpha} \frac{\partial \rho_g}{\partial \eta_{\alpha i}} \frac{\partial \eta_{\alpha i}}{\partial t}\right]$$

Vacancies:

$$\frac{\partial \mu_v}{\partial t} = \frac{1}{\chi_v}\left[\nabla \cdot (D_v \chi_v \nabla \mu_v) + s_v - \sum_{\alpha}\sum_{i=1}^{p_\alpha} \frac{\partial \rho_v}{\partial \eta_{\alpha i}} \frac{\partial \eta_{\alpha i}}{\partial t}\right]$$

Phase-field model initial conditions

- Intergranular bubble areal density (n_a): Determine from rate theory simulations
  - At 1035 K, n_a = 15 / μm^2

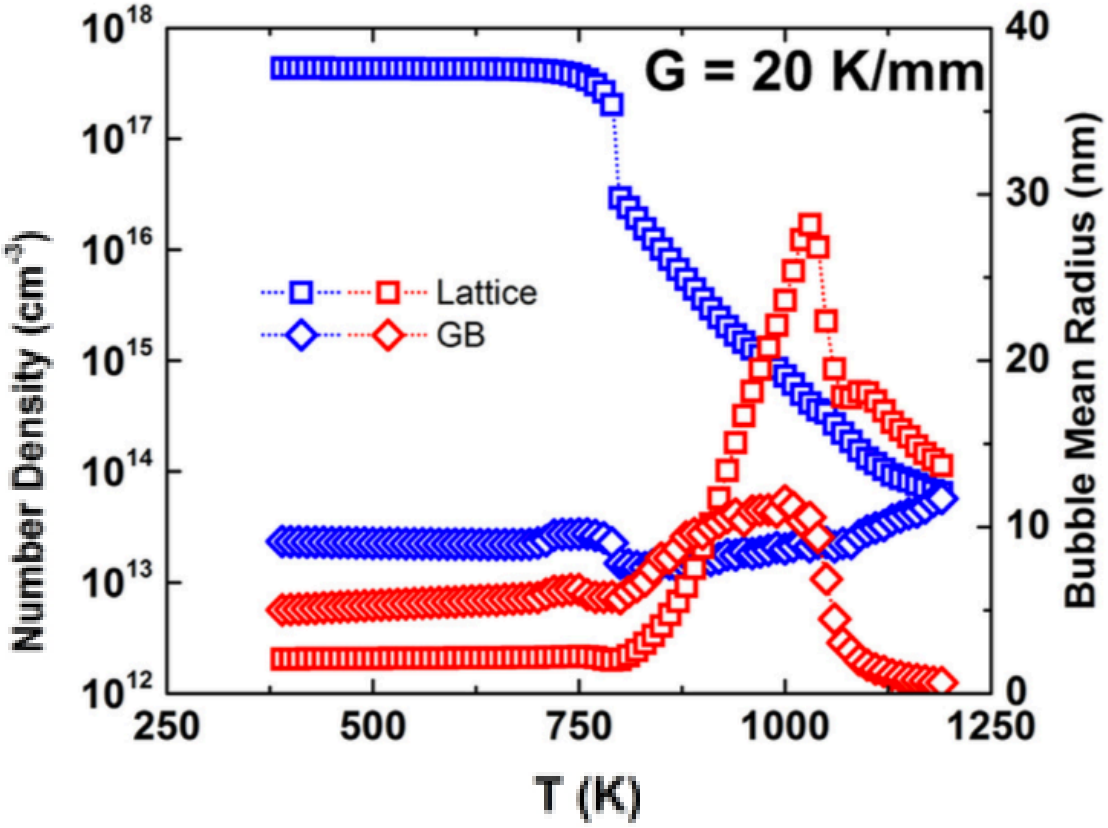

Y. Miao, K.A. Gamble, D. Andersson, B. Ye, Z.-G. Mei, G. Hoffman, A.M. Yacout, *Nucl. Eng. Design,* 322, 336-344 (2017).

Phase-field simulation results

- Determine $F_{c,sat}$
- 1035 K
- $\theta/2 = 73$
- No-flux boundary conditions
- 3 μm × 3 μm grain boundary
- Populate with randomly placed lenticular bubbles, n_a = 15 / μm^2, minimum spacing 160 nm

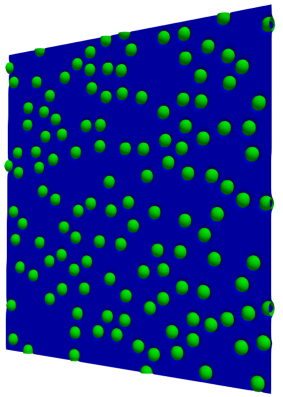

$t = 0$

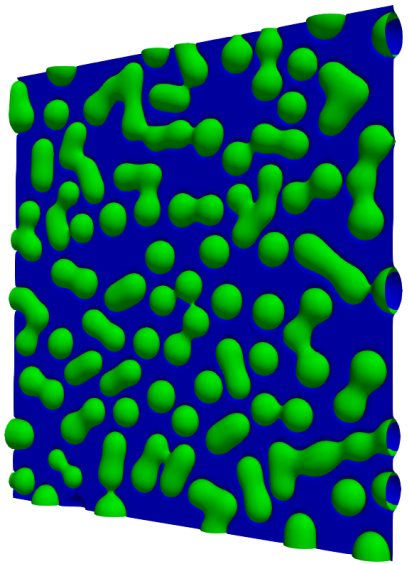

$t = 6.04 \times 10^7$ s

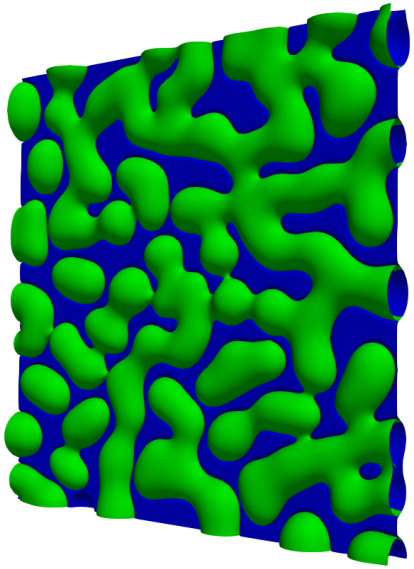

$t = 1.62 \times 10^8$ s

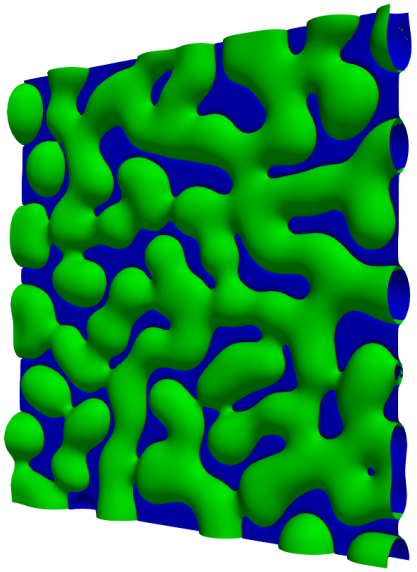

$t = 1.97 \times 10^8$ s

Phase-field simulation results

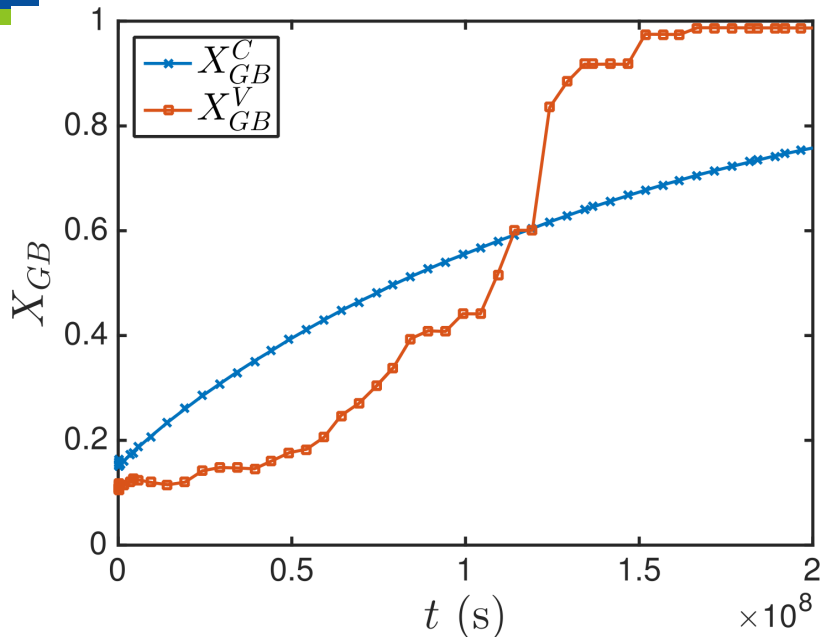

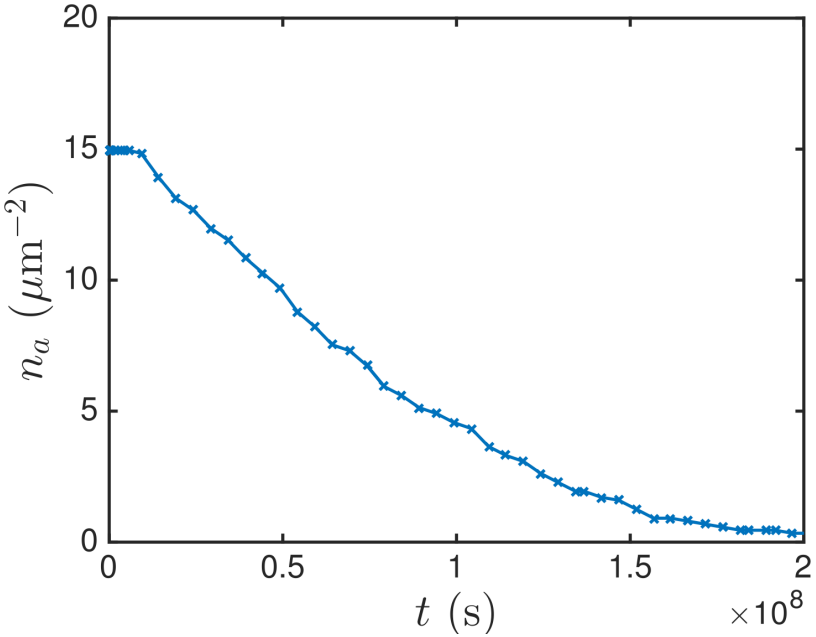

- Plot fractional coverage of GB (X_{GB}^C) and fraction of bubbles that are vented to edge of domain (X_{GB}^V) vs. time
  - Less rapid increase with respect to time compared to previous simulations of Millett et al., due to to slow buildup from source terms
- Areal density of bubbles vs. time
  - Rate of coalescence relatively constant until the bubble density reaches approximately half its initial value, then slows

Effect of minimum bubble spacing in initial conditions

- Also simulated l_{min} = 130 nm, 200 nm, 5 configurations each
- 200 nm: Initial portion of release curve delayed
- Slight decrease in $F_{c,sat}$ with l_{min}, but may be just due to statistical variation

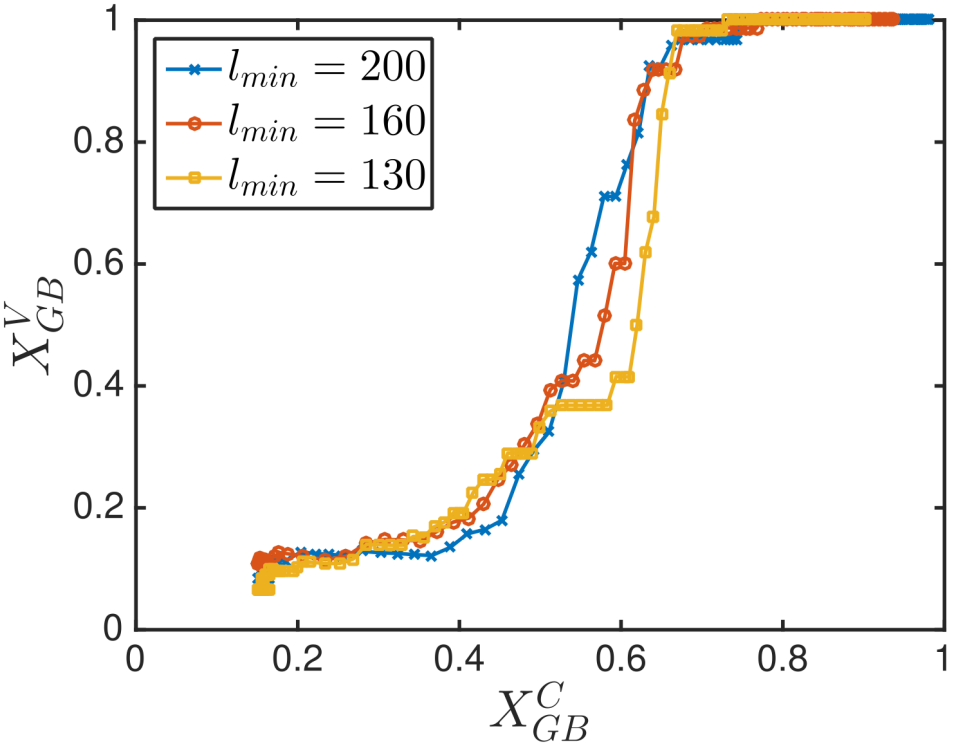

Min. spacing (l_{min}), nm	$F_{c,sat}$
130	0.61 ± 0.039
160	0.60 ± 0.036
200	0.58 ± 0.046

Effect of simulation temperature

- Current BISON model assumes $F_{c,sat}$ is independent of temperature
- Primary effect of varying temperature: Gas diffusivity D_g
- Ran 5 simulations with T = 1015 K (D_g decreased by 2x)
  - Much finer microstructure at same simulation time
  - No change in calculated $F_{c,sat}$ = 0.60 ± 0.014

Microstructure at
$t = 1.98 \times 10^8$ s:

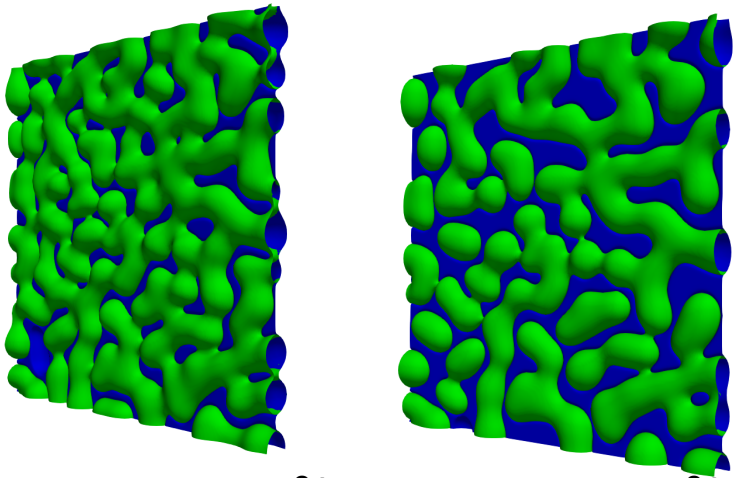

$D_g = 0.05$ nm^2/s $D_g = 0.1$ nm^2/s

Informing BISON with phase-field results

- Plot fraction of bubbles that are vented to edge of domain (X_{GB}^V) vs. fractional coverage of GB (X_{GB}^C)
- Implications for BISON:
  - Short term: Set $F_{c,sat}$ where slope of curve is greatest (shown: $X_{GB}^C = 0.62$)
  - Longer term: Modify BISON model to turn off swelling and release gas gradually following curve shape

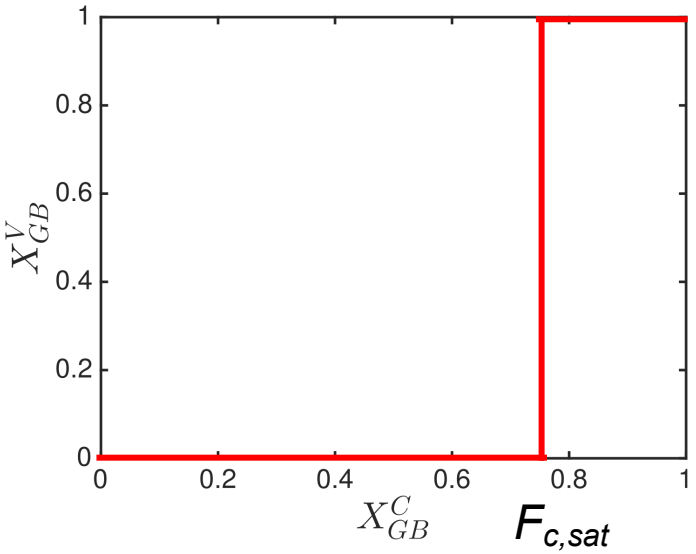

Previous BISON Assumption

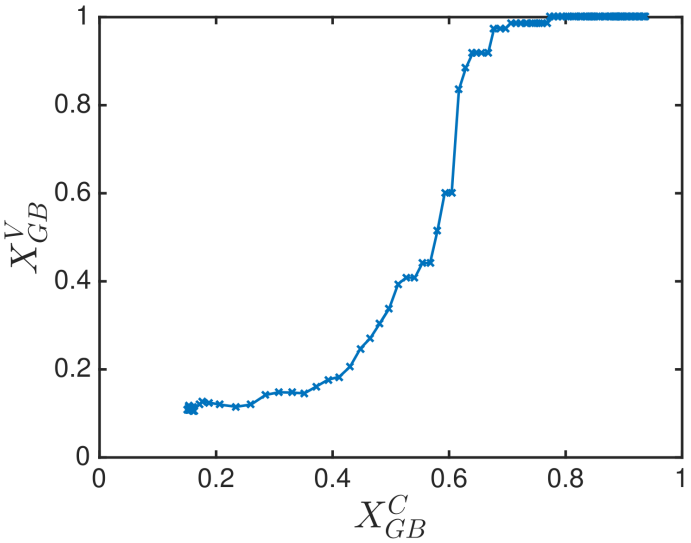

Marmot Simulation

Effect of simulation assumptions on predicted value for BISON model

- Simulation initial conditions
  - Maintain all simulation parameters the same, including minimum spacing l_{min} = 160 nm
  - Change seed in random number generator used to determine initial bubble positions
  - 5 total configurations simulated using these parameters
- Mean $F_{c,sat}$ = 0.60
- Standard deviation indicates calculated value of $F_{c,sat}$ is relatively insensitive to initial bubble configuration

Configuration	$F_{c,sat}$
1	0.54
2	0.62
3	0.61
4	0.63
5	0.62
Mean	0.60
Standard Deviation	0.036

Effect of simulation domain geometry

- Compare venting curves for circular GB vs. square GB
  - Circular GB: $F_{c,sat}$ = 0.61 ± 0.046, Square GB: 0.60 ± 0.036
  - Conclude that GB geometry does not have a significant effect

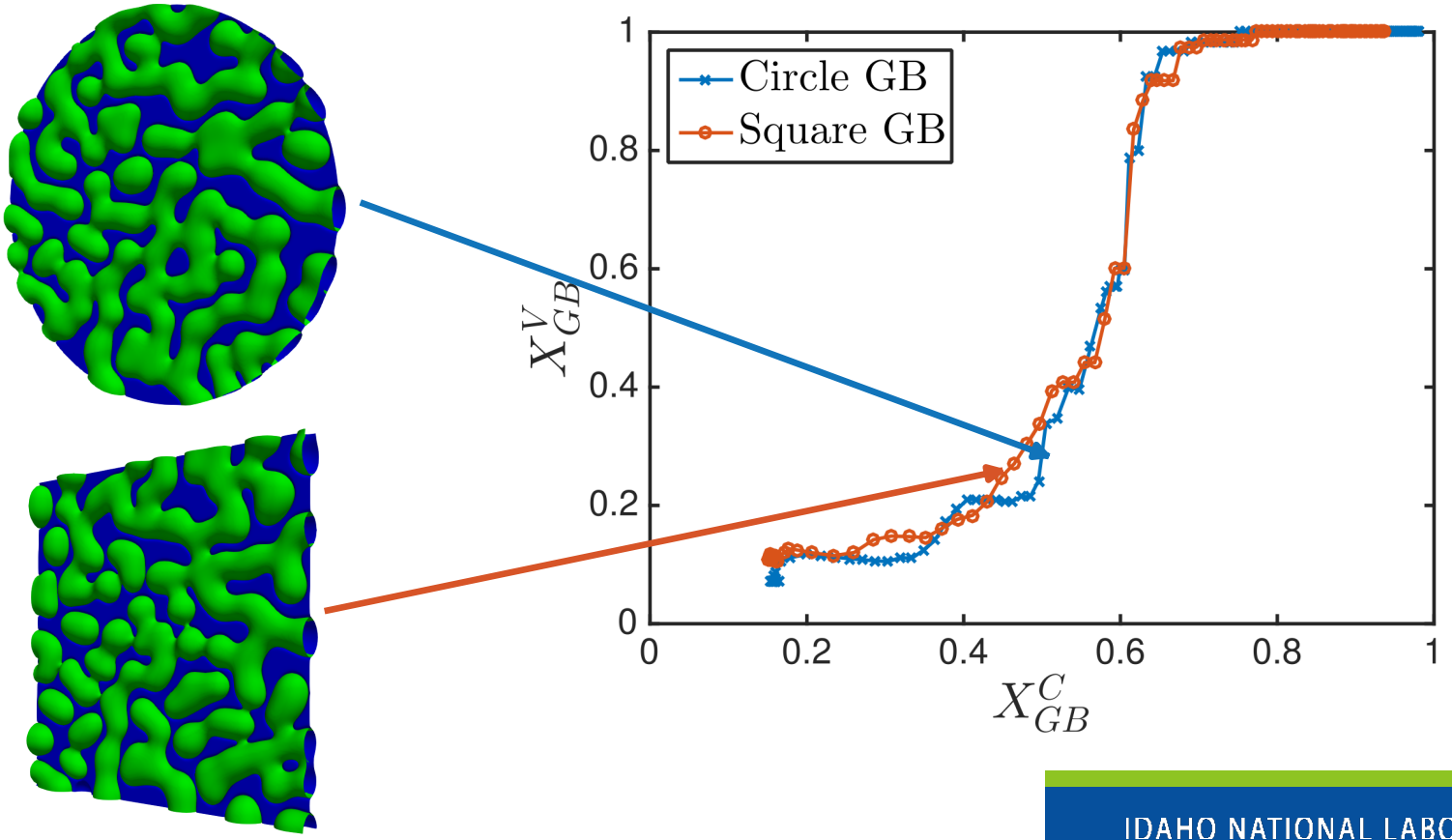

BISON simulations using updated $F_{c,sat}$

- Meso-scale informed BISON model used to simulate U3Si2 rodlets irradiated in Advanced Test Reactor at INL
  - ATF-13 R4, ATF-15 R6
- Experimental FGR in range of BISON prediction
- Significantly reduced uncertainty in FGR prediction (caveat: different rodlets)
- Model performance significantly improved

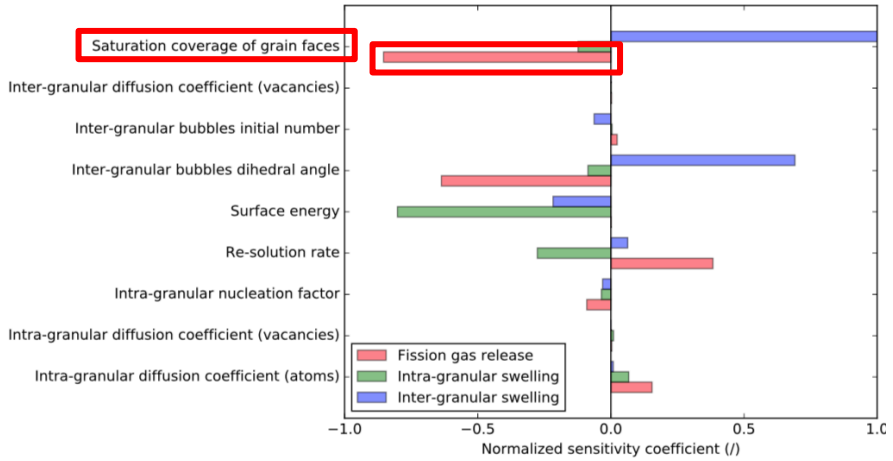

$0.5 < F_{c,sat} < 0.78$

Barani et al., JNM, 522, 97-110 (2019)

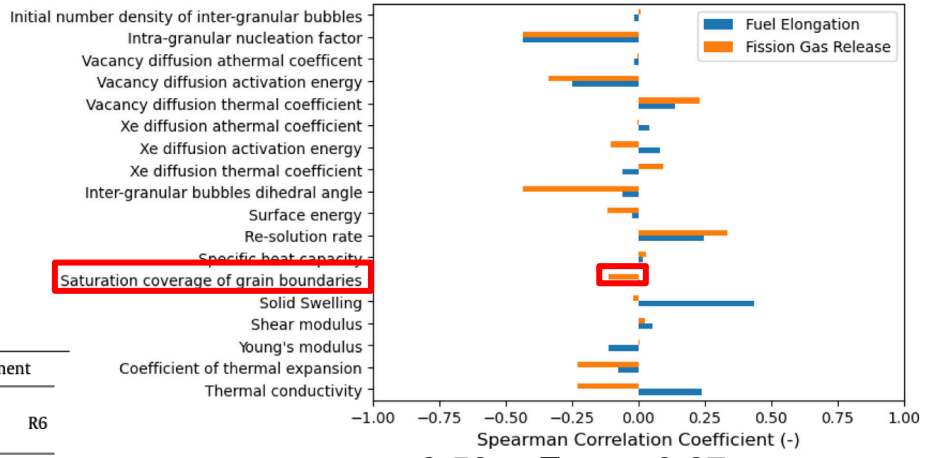

$0.53 < F_{c,sat} < 0.67$

Gamble et al., JNM, 555, 153097 (2021)

	BISON				Experiment	
	R4		R6		R4	R6
	Stoichiometric	Si-Rich	Stoichiometric	Si-Rich		
Fuel elongation (mm) (this work)	0.067 to 0.195	0.055 to 0.187	0.091 to 0.267	0.055 to 0.282	0.0	0.0
Fission gas release (/) (this work)	0.0 to 0.011	0.0 to 0.004	0.0 to 0.020	0.0 to 0.018	0.0006	0.0006
Fuel elongation (mm) [16]	-0.135 to 0.132	-0.131 to 0.057	N/A	N/A	0.0	0.0
Fission gas release (/) [16]	0.0 to 0.014	0.0 to 0.009	N/A	N/A	0.0006	0.0006

Conclusions: U_3Si_2 fission gas release

- Used atomistic and mesoscale methods together to answer questions for engineering-scale fuel performance modeling
  - Phase-field simulations were used to calculate $F_{c,sat}$
  - Determined without needing to wait for costly post-irradiation examination
  - No strong effect on $F_{c,sat}$ from initial conditions, minimum bubble spacing, simulation domain geometry, temperature (in range considered)
- New value of $F_{c,sat}$ was used in BISON simulations of U_3Si_2 irradiated in the Advanced Test Reactor at INL
  - Reduced uncertainty in fission gas release predictions

Introduction: Electric-Field Assisted Sintering (EFAS)

- Technique for powder consolidation using simultaneous application of heat, pressure, electric field
- Allows consolidation of powders (metal, ceramic) with lower energy input compared with hot pressing
- Potential applications relevant to Idaho National Lab (INL)'s mission:
  - Nuclear fuel pellets, moderator and reflector materials, heat exchangers, hydrogen production
- INL is investing in experimental and modeling & simulation capabilities to study EFAS. Test case: Y_2O_3
  - Modeling microstructural evolution: Phase-field

DCS-800

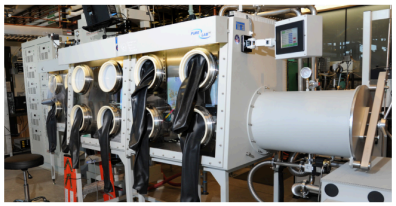

Rad EFAS

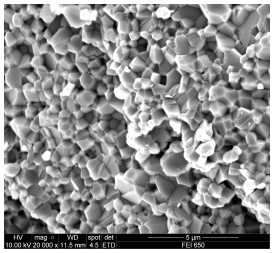

EFAS Y_2O_3

MALAMUTE: Mod-sim of Advanced Manufacturing

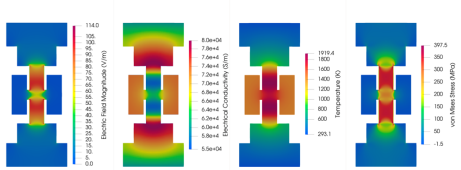

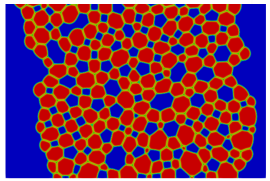

Microstructure in the Phase-field Model

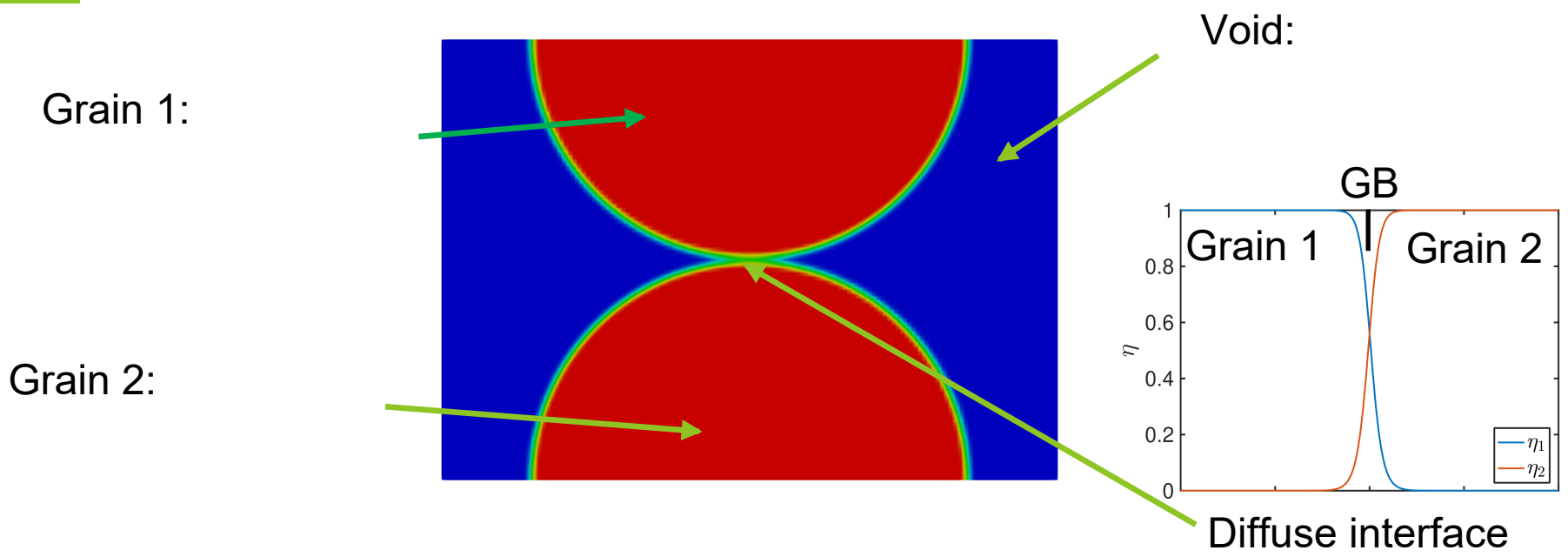

- Order parameters represent grains of the solid Y_2O_3
- Order parameter represents the void phase
  - Diffuse interface between order parameters represents grain boundaries (GBs), surfaces, usually wider than physical width
- Vacancy species and, corresponding densities and
  - Void phase composed entirely of vacancies

Phase-Field Model: Grand-Potential Functional

$$\Omega = \int_V \left(m \left[\sum_\alpha \sum_{i=1}^{p_\alpha} \left(\frac{\eta_{\alpha i}^4}{4} - \frac{\eta_{\alpha i}^2}{2} \right) + \sum_\alpha \sum_{i=1}^{p_\alpha} \left(\sum_\beta \sum_{j=1, \alpha i \neq \beta j}^{p_\beta} \frac{\gamma_{\alpha i \beta j}}{2} \eta_{\alpha i}^2 \eta_{\beta j}^2 \right) + \frac{1}{4} \right] + \frac{\kappa}{2} \sum_\alpha \sum_{i=1}^{p_\alpha} |\nabla \eta_{\alpha i}|^2 + \sum_\alpha h_\alpha \omega_\alpha \right) dV$$

- Multi-phase, multi-order parameter extension to grand-potential model[1]. Grand potential of solid phase: $\omega_s = f_{ec,s} - \mu_{V_Y} n_{V_Y}^s - \mu_{V_O} n_{V_O}^s - \vec{D} \cdot \vec{E}$
- Advantages:
  - Bulk free energy contribution is removed from interfacial energy
  - Allows interfacial thickness and energy to be set independently, enabling coarser mesh, improved computational performance
  - Similar to KKS in this respect, but do not need separate phase concentration variables, so performance is improved
  - Prevents spurious formation of additional phases at two-phase interfaces

[1] L.K. Aagesen, Y. Gao, D. Schwen, K. Ahmed, *Phys. Rev. E*, 98, 023309 (2018).

Evolution Equations

- Allen-Cahn Equations for Order parameters:

$$\frac{\partial \eta_i}{\partial t} = -L_s \frac{\delta \Omega}{\delta \eta_i} \qquad \frac{\partial \phi}{\partial t} = -L_v \frac{\delta \Omega}{\delta \phi}$$

- Vacancy concentration evolution: Chemical Potential

$$\chi_{V_Y} \frac{\partial \mu_{V_Y}}{\partial t} = \nabla \cdot \chi_{V_Y} \mathbf{D}_{V_Y} \nabla \mu_{V_Y} - \left(\frac{\partial n_{V_Y}}{\partial \phi} \frac{\partial \phi}{\partial t} + \sum_i \frac{\partial n_{V_Y}}{\partial \eta_i} \frac{\partial \eta_i}{\partial t} \right)$$

- Vacancy diffusivities higher at GBs (10^6), surfaces (10^9)
- Electric potential: split into equilibrium potential and homogeneous solution (deviation due to applied E-field)

$$\frac{\delta \Omega}{\delta V} = 0 \qquad \frac{\partial \rho}{\partial t} = \nabla \cdot s \nabla \delta v \approx 0 \qquad s = \sum_i \frac{e^2 Z_i^2 n_i D_i}{kT}$$

- Joule heating:

$$\dot{q} = s \left| \nabla \delta V \right|^2$$

Defect segregation to Grain Boundaries: 1D

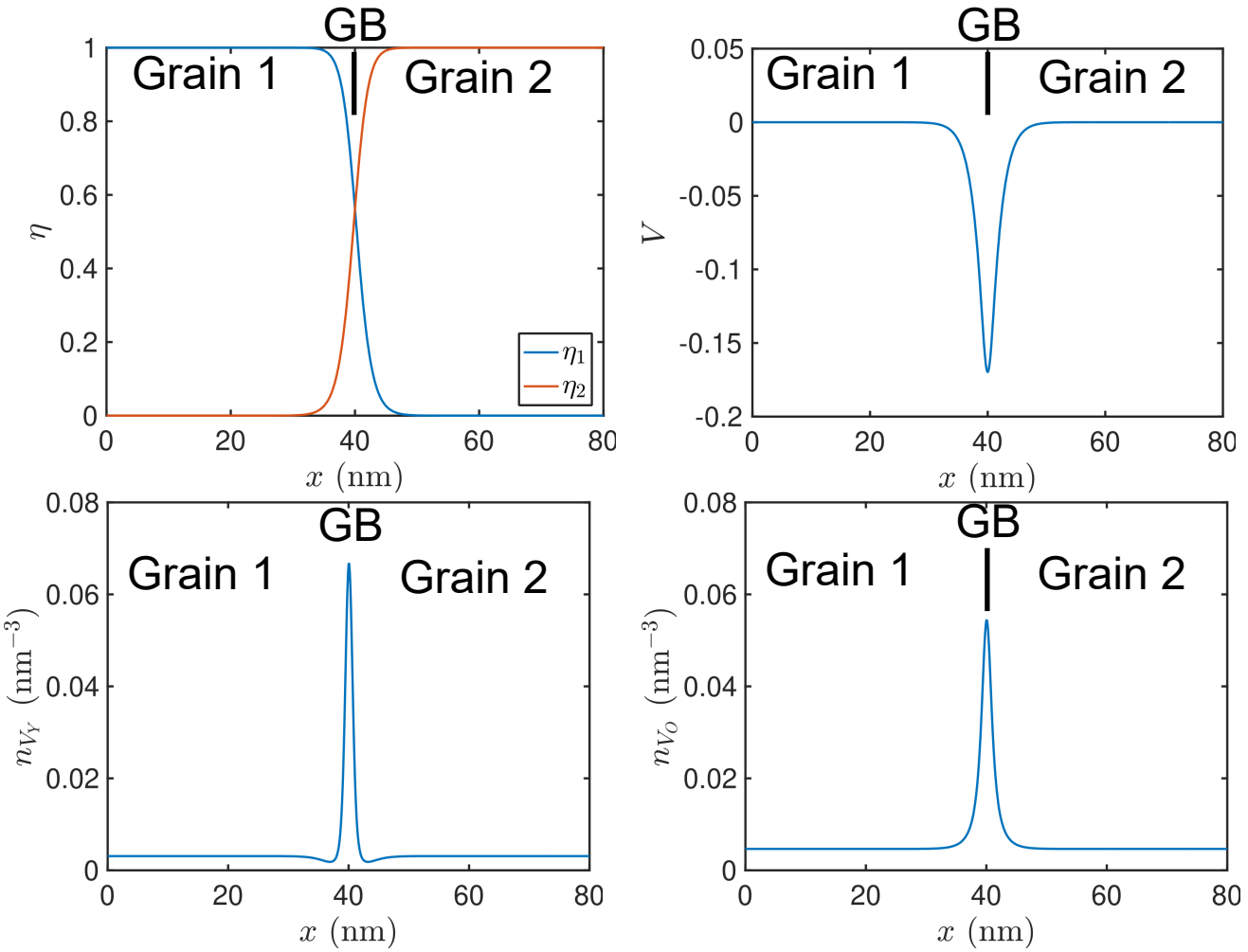

- Lower formation energies at GBs gives elevated vacancy concentrations, charge imbalance
  - Results in electric potential difference

Microstructure evolution and neck growth of two-particle contact

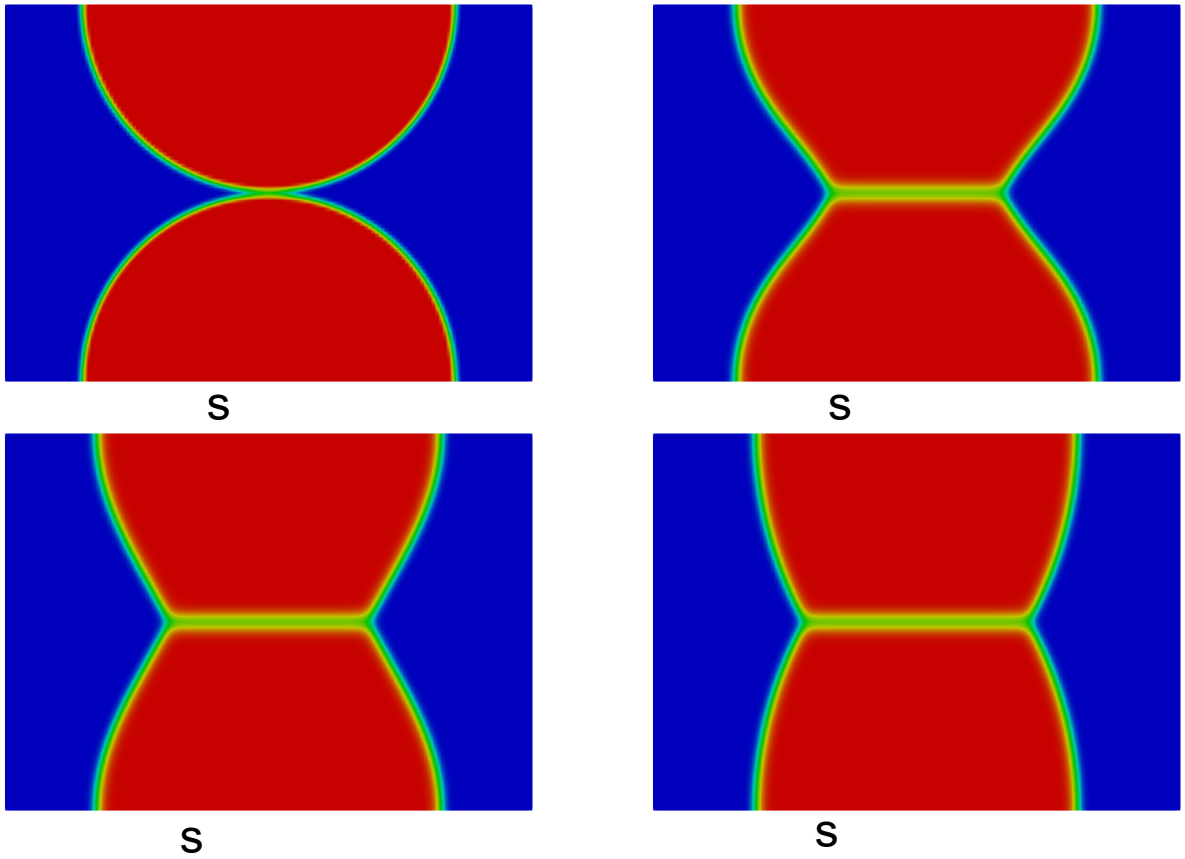

- Two particles in contact with initial particle radius
  - Varying initial radius R and applied E-field, initial T = 1600 K
  - Shown here: R = 50 nm and E = 4000 V/m

Enhanced electrical conductivity and heat generation along surfaces, GBs

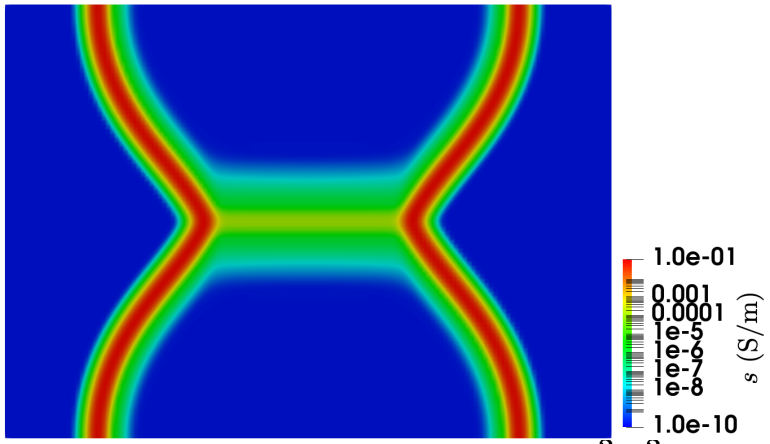

Electrical conductivity: $s = \sum_i \frac{e^2 Z_i^2 n_i D_i}{kT}$

s

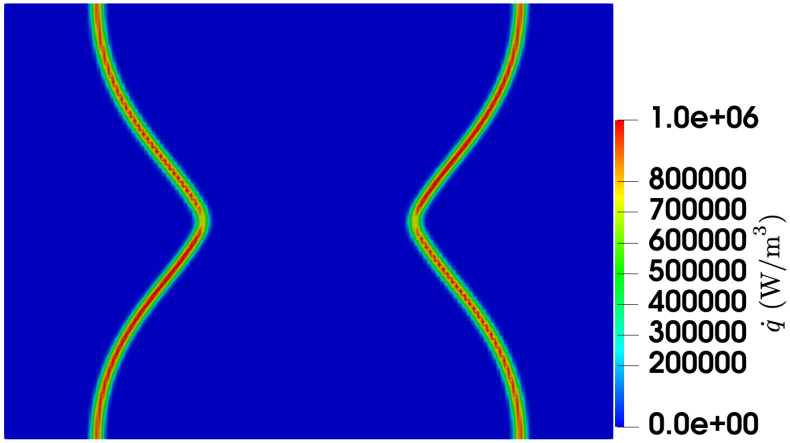

Heat generation: $\dot{q} = s\,|\nabla \delta V|^2$

s

- Electrical conductivity enhanced at surfaces, grain boundaries due to enhanced defect diffusivity
- Local heat generation primarily located to surfaces in this geometry due to surface enhancement of diffusivity
- Heat redistributes very rapidly in particles compared to time scale of EFAS process
  - Assume local temperature rise can be found from volume-average of heat generation at each

Neck grows faster for smaller particles

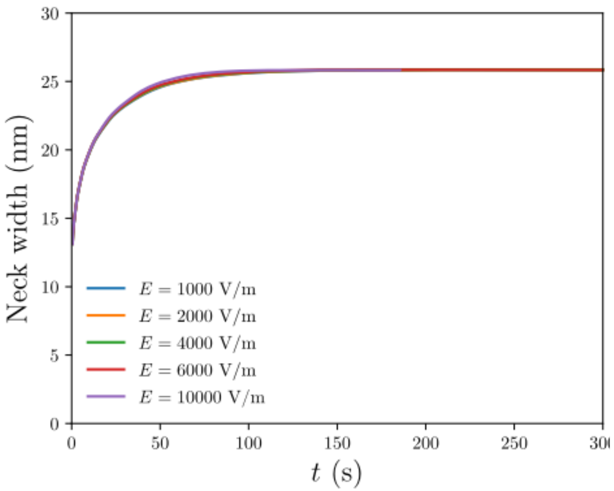

Initial nm

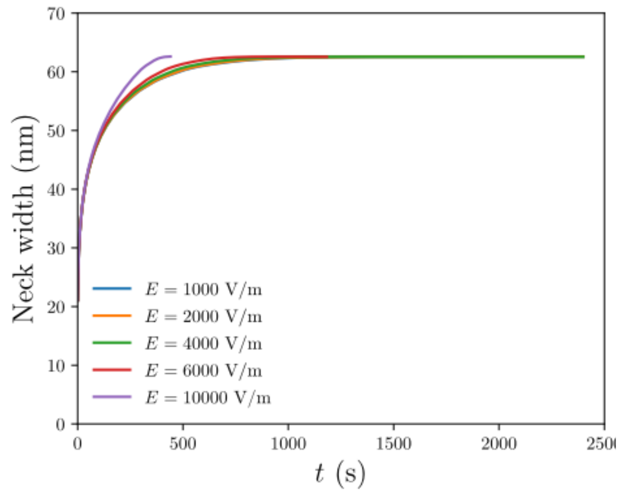

Initial nm

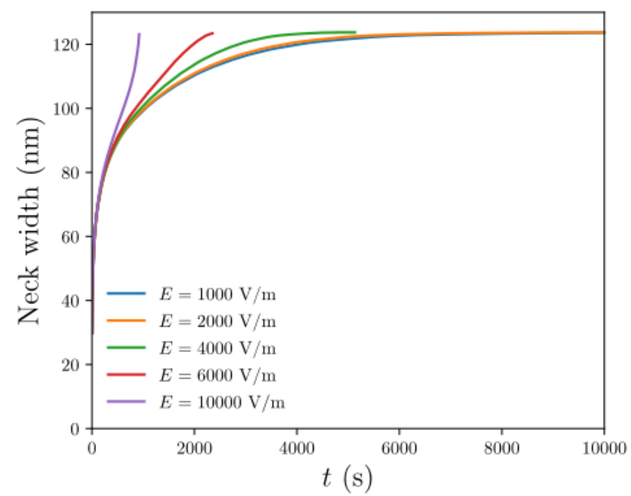

Initial nm

- Increasing E-field causes acceleration of neck growth for larger particles

Onset of flash: Temperature spike occurs for larger E-field

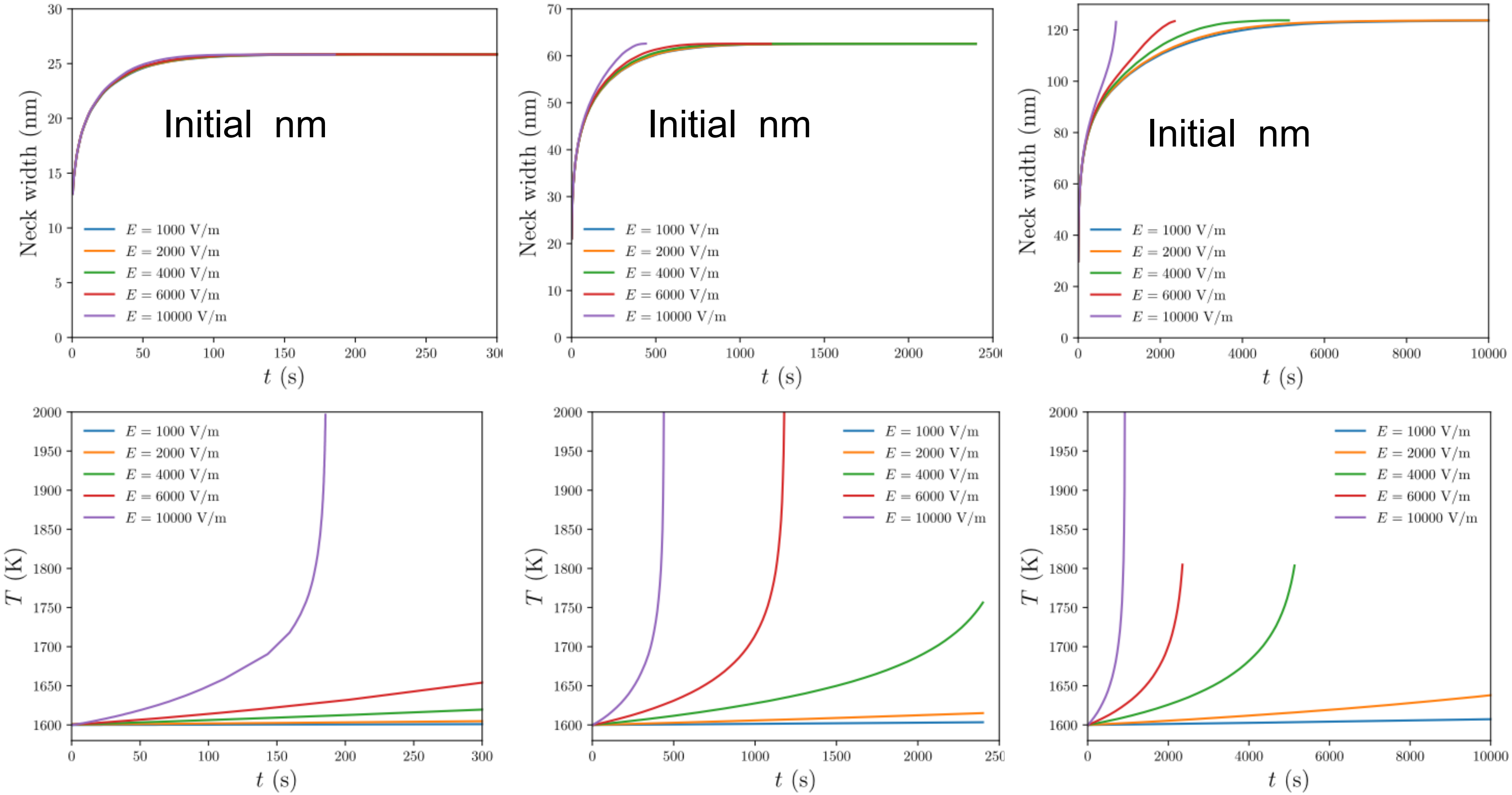

- E-field causes temperature spike sooner relative to neck growth for larger particles

Many-particle simulations

- Initial radius nm, V/m

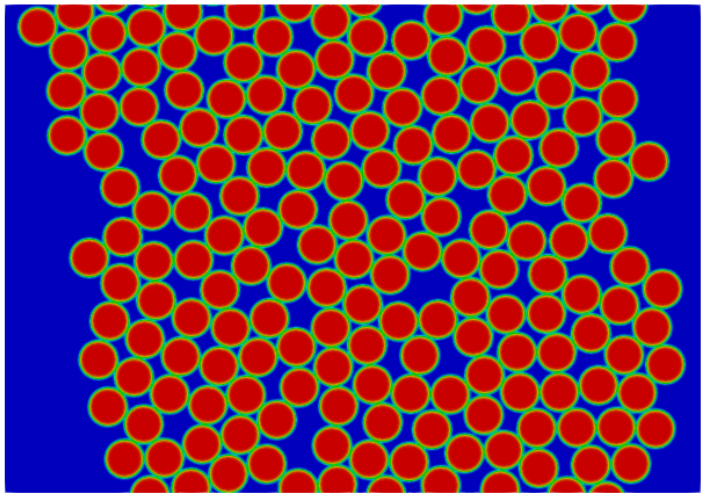

s

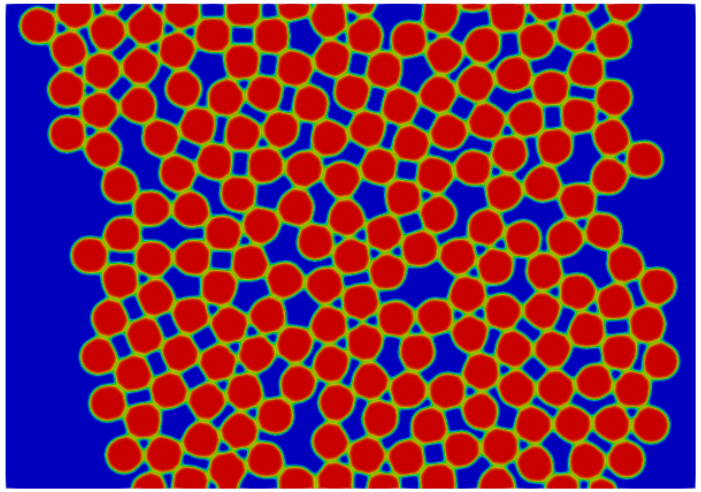

s

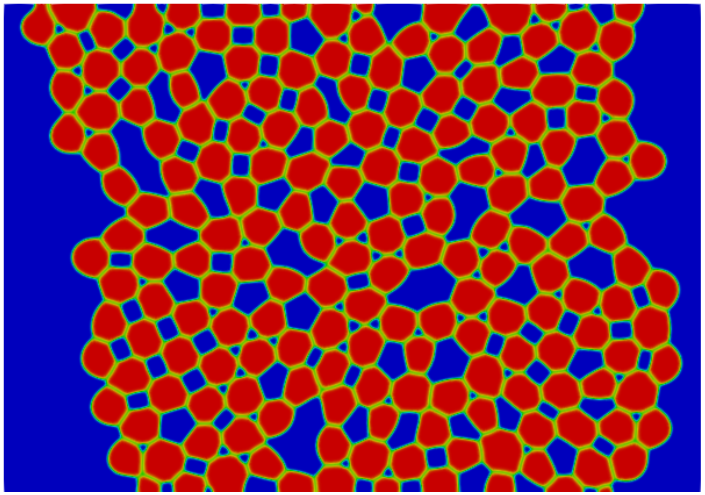

s

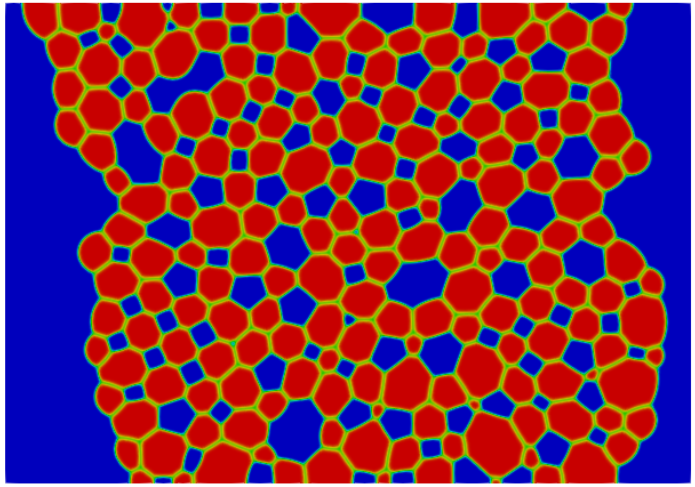

s

Conductivity and heat generation

- Grain structure overlaid in black
- Enhanced conductivity on surfaces, GBs
  - Highest conductivity on internal, external surfaces
- Highest heat generation rate on external surfaces
- Many significant localized heat spots internally

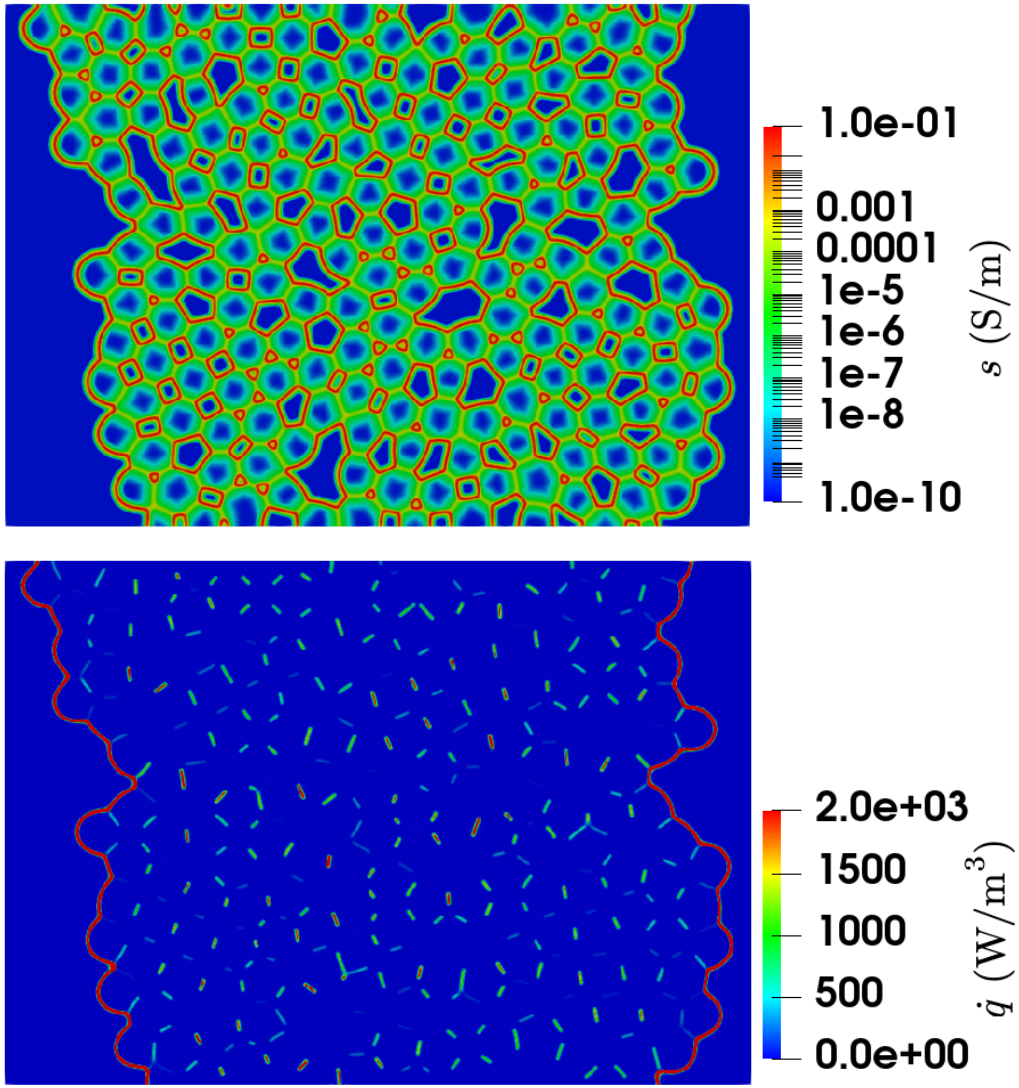

Internal heat generation

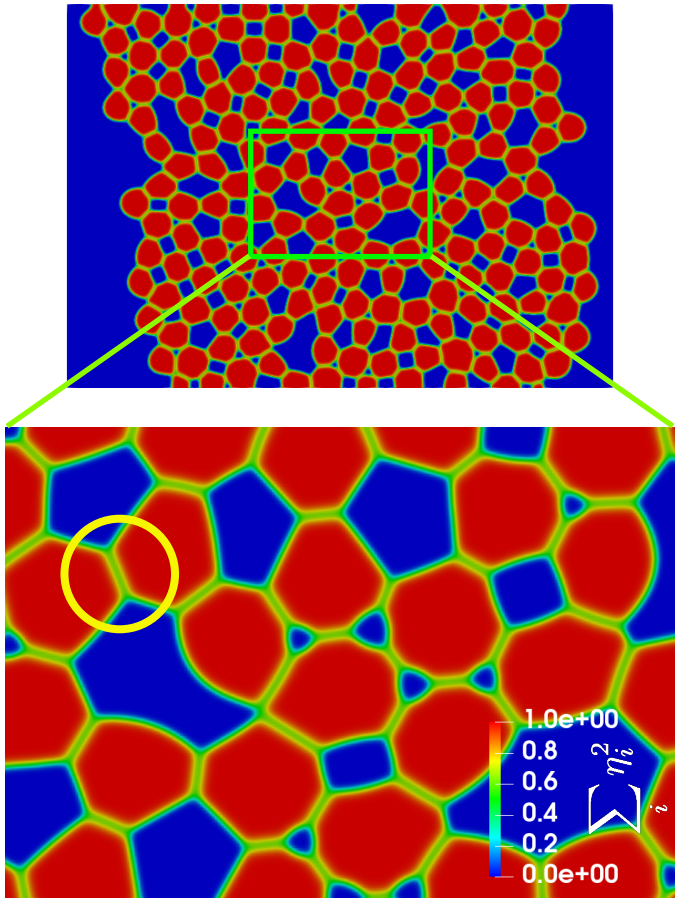

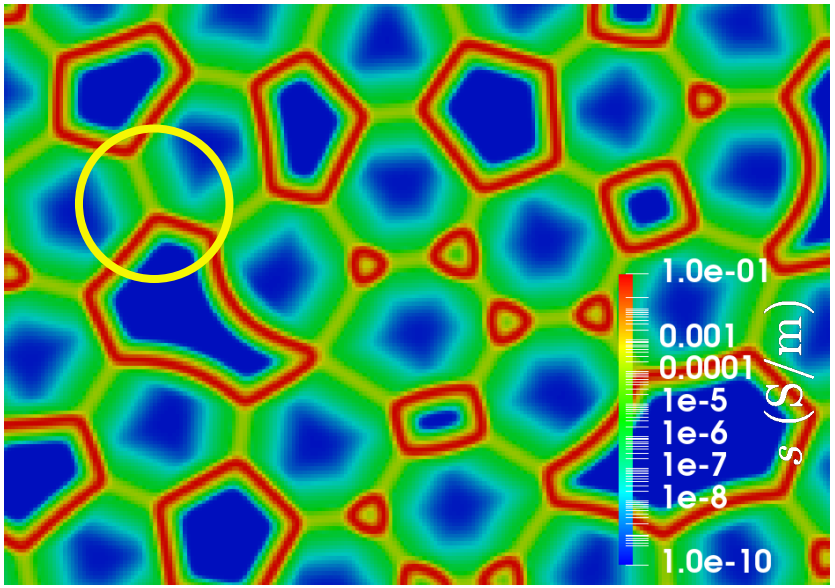

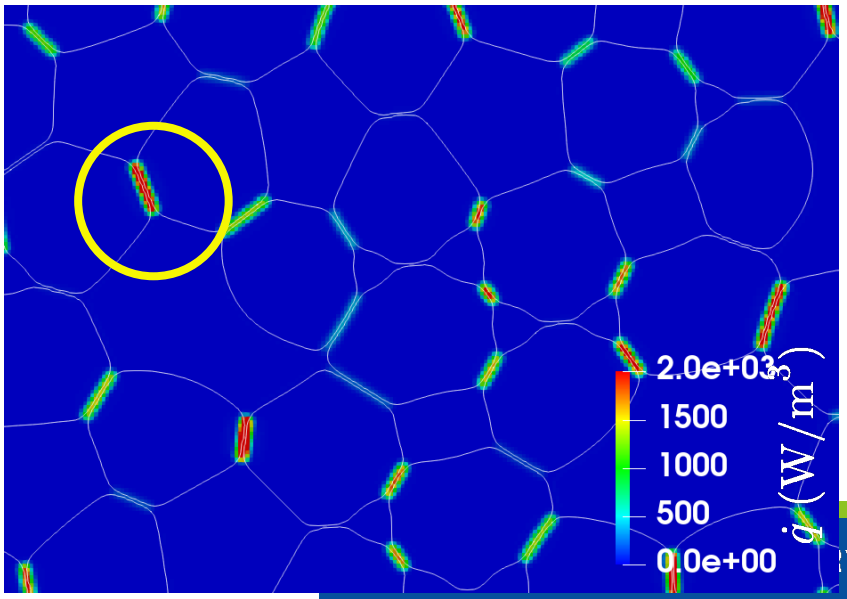

- Grain structure overlaid in white
- Although conductivity is much higher on internal surfaces than GBs, internally, heat generation is localized to GBs-?

Internal heat generation

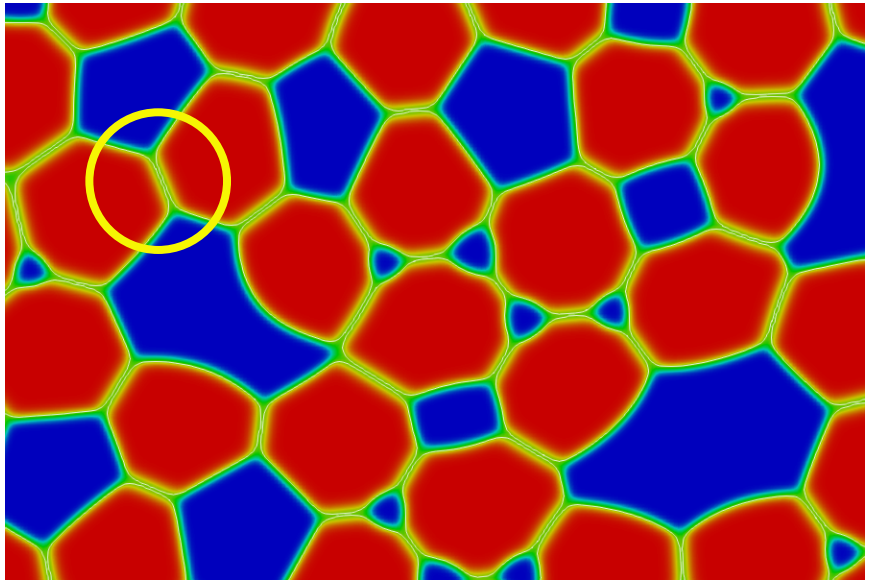

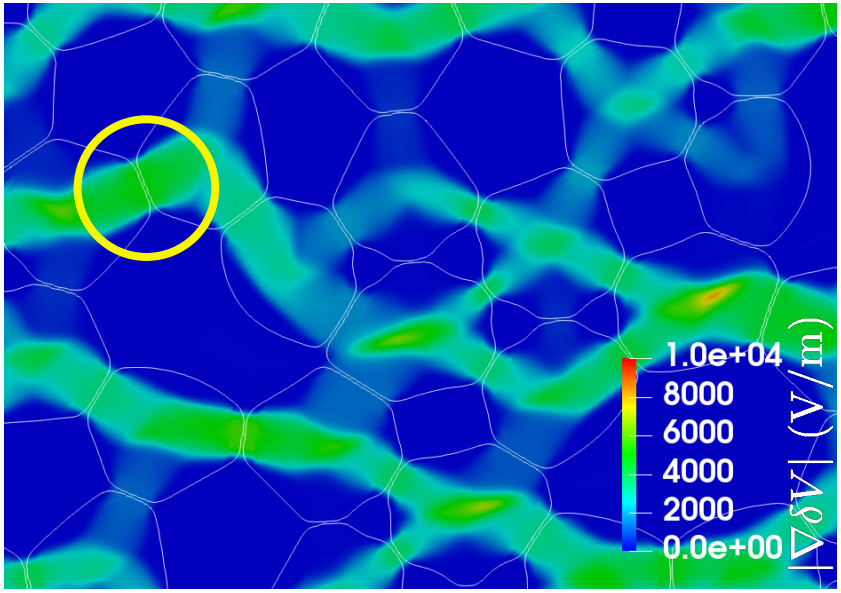

- Applied potential drop localized to grain boundaries
- Since $\dot{q} = s\,|\nabla \delta V|^2$, drop in dominates
- In experiments, area of surface pathway is smaller, so generation at GBs should dominate

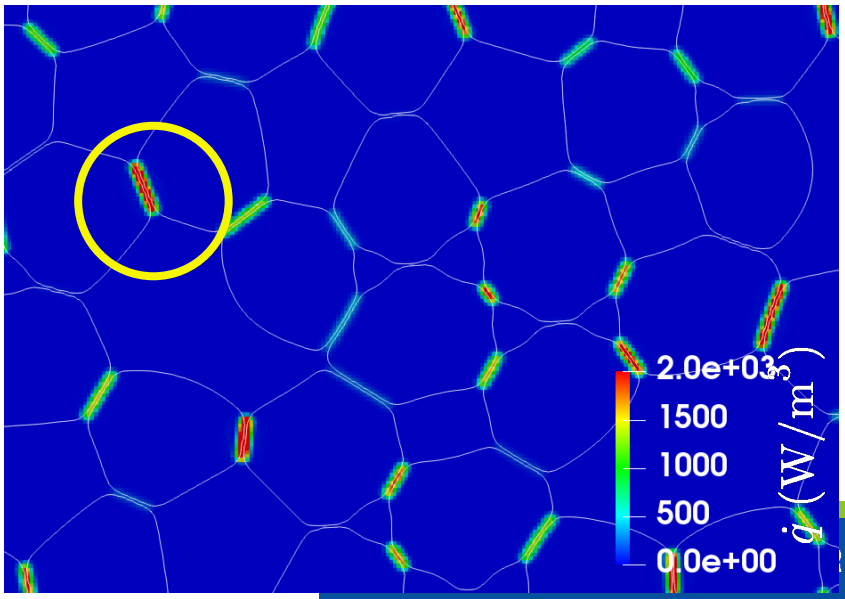

Multi-scale simulation Framework

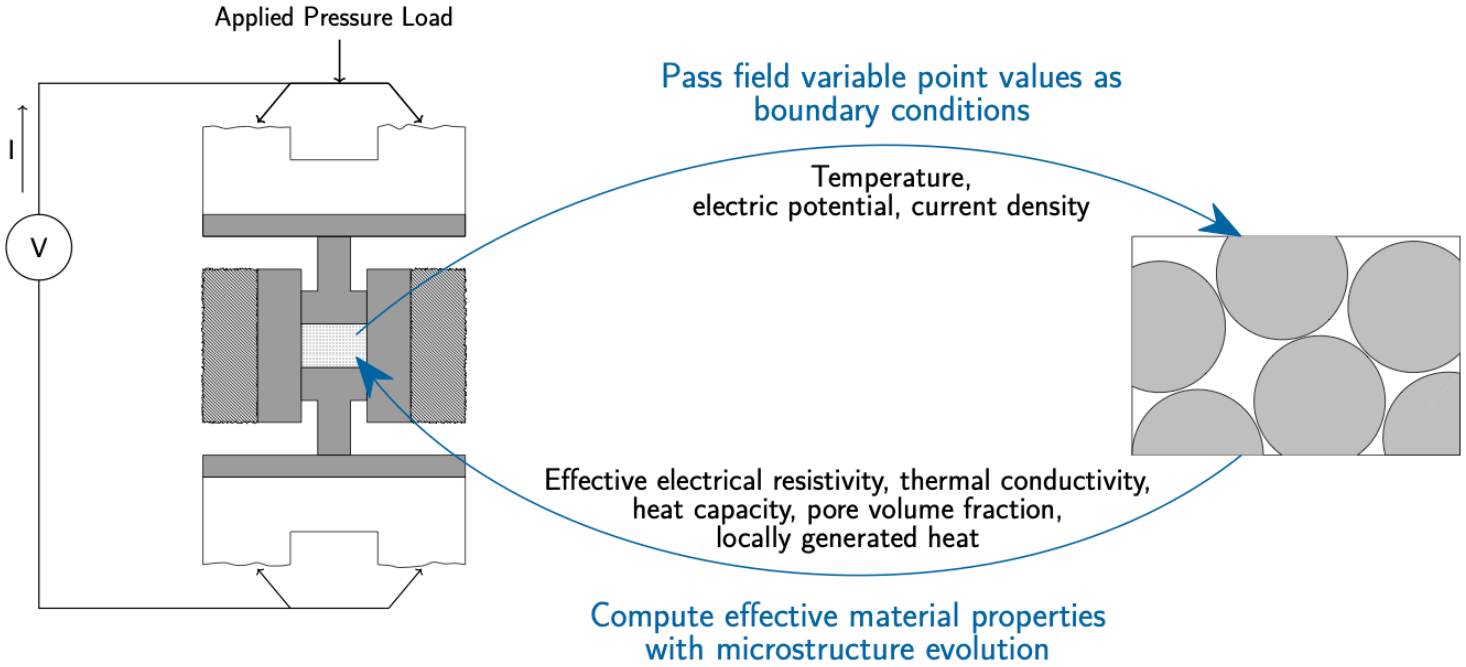

Single Engineering Scale Simulation

Multiple Representative Microstructure Simulations

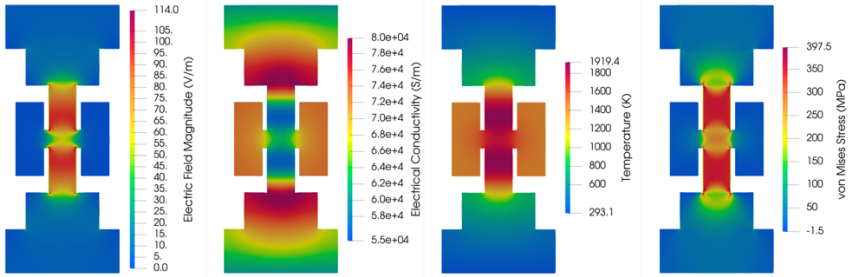

MALAMUTE

Conclusions: Electric Field Assisted Sintering

- Developed phase-field model of EFAS process that accounts for grain structure, defect species, electric field due to charged defects and applied electric field
  - Computationally efficient due to grand potential formulation
  - Extensible to other materials and arbitrary number of defect species
- Simulated neck growth rate in 2-particle configuration
  - Applied E-field has increasing impact for larger particles
- Simulated multi-particle configuration
  - Internal Joule heating localized to GBs
- Multi-scale framework linking engineering to meso-scale
- Future work:
  - Integrate plastic flow effects into electrochemical phase-field model, validate
  - Run multi-scale process simulations, validate

Irradiation-Driven Defect Superlattice Formation in Metals and Alloys

- Ordered array of defects
- Ion or fission neutron irradiation
  - Void superlattice: 5-20 nm diameter, 20-80 nm superlattice parameter
  - Gas bubble superlattice (GBS): 2-4 nm diameter, 5-10 nm superlattice parameter
- Superlattice (usually) has same structure as material's crystal structure
- Hypotheses on formation mechanism:
  - Dislocation-cavity interaction
  - Turing Instability
  - Elastic constant anisotropy
  - 1D, 2D interstitial diffusion
- Practical and fundamental scientific interest
  - Improved fission gas retention for fuel
  - Modify transport properties, i.e. photonics or plasmonics?

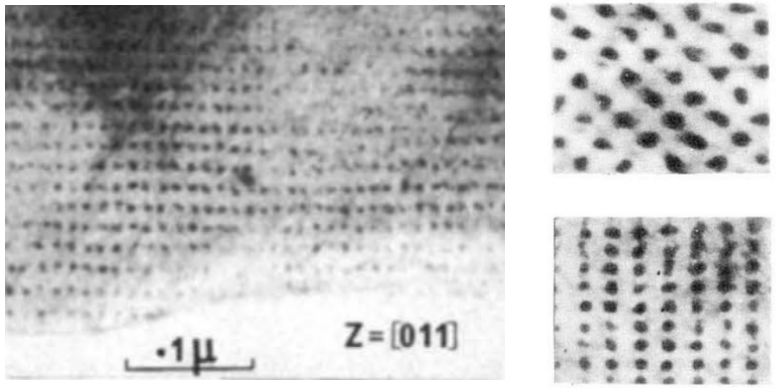

Void superlattice in BCC Mo

Evans et al., Nature, 229, p. 403 (1971)

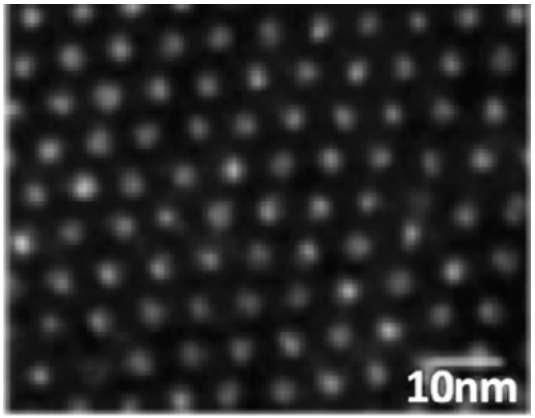

Fission GBS in BCC U-Mo

Gan et al, JNM, 396, p. 234 (2010)

Void Superlattice Formation: Phase-Field Simulations

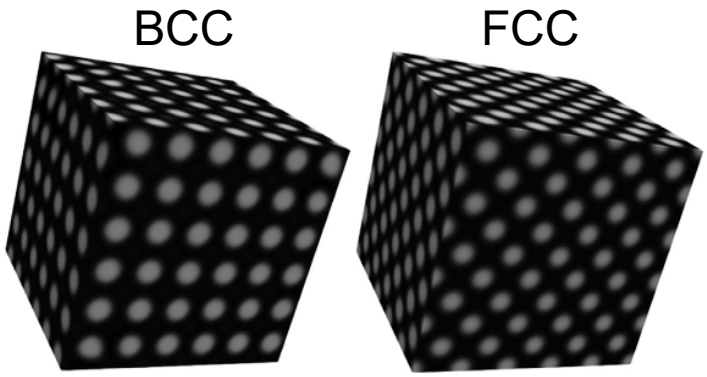

Diffusion anisotropy

Gao et al, Materialia, 1, p. 78 (2018)

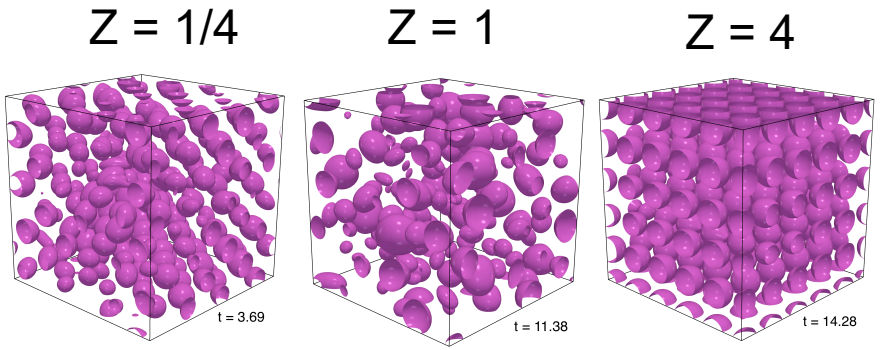

Elastic anisotropy

Gao et al, Comp. Mat. Sci., 206, p. 111252 (2022)

- Cahn-Hilliard equation for vacancy evolution
- Diffusion equation for self-interstitial atoms (SIA)
- Production, recombination terms
- Anisotropic interstitial diffusion
  - BCC: 4 interstitial species, <111>
  - FCC: 6 interstitial species, <110>
  - Nucleation or spinodal decomposition
  - **Simulated microstructures match underlying crystal structure**
- Elastic constant anisotropy
  - Defect eigenstrain in matrix
  - Varying Zener anisotropy ratio
  - FCC for , simple cubic for
  - **Not consistent with experimentally observed superlattice microstructures**
  - **BCC superlattices form in tungsten (Z=1)**
- **Evidence points to diffusion anisotropy**

Unified Phase-Field Model for Void and Gas Bubble Superlattice Formation

- Grand potential functional
  - Solid and void/bubble phases
  - Defects: vacancies, interstitial gas atoms, SIA (1D diffusivity)
  - Production, vacancy-SIA recombination, sink absorption
- Model can capture void/bubble formation by spinodal decomposition or nucleation
  - Based on experimental observations, focus on nucleation
  - Introduce nuclei at rate based on classical nucleation theory
  - Forcing function added to order parameter for void/bubble phase for a fixed “hold time”:
  - Vacancies flow to nucleus to stabilize it, then forcing function turns off
  - Local mesh refinement at nucleus position

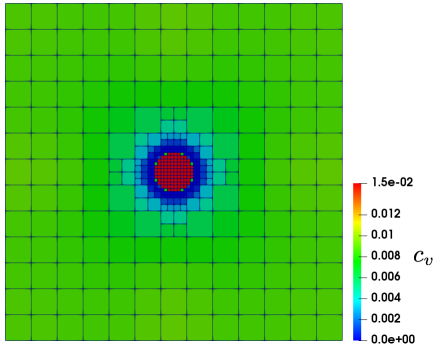

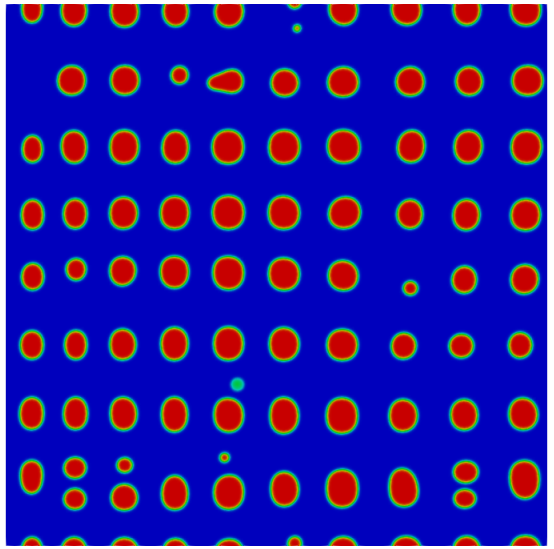

Effect of parameters on superlattice morphology

- Two-point correlation function used to determine superlattice spacing
- Void superlattice spacing:
  - Decreases with nucleation rate
  - Increases with vacancy diffusivity
  - Decreases with defect production
- Gas bubble superlattice spacing
  - ☑ Constant with increasing fluence
  - ☑ Decreases with gas atom flux
  - ✕ Increases with increasing gas/vacancy ratio: not accounting for bound gas-vacancy cluster, which decrease cluster diffusivity

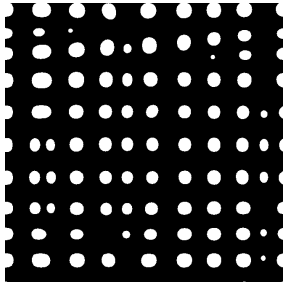

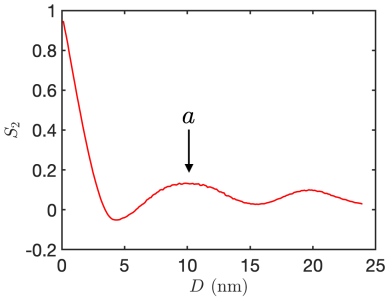

Voids

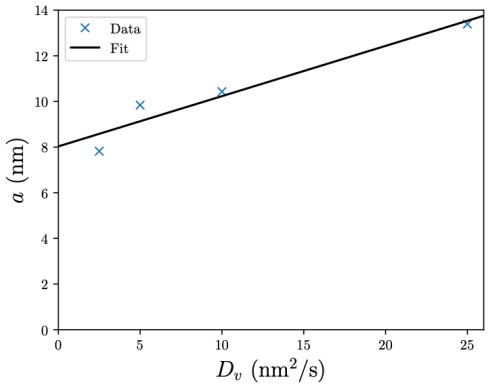

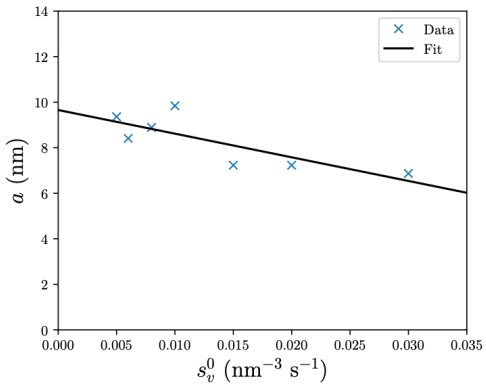

Gas bubbles

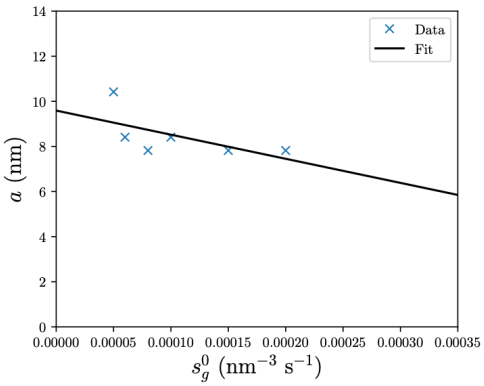

Superlattice formation in W-Re alloys

- BCC superlattice forms in pure W (elastically isotropic)
- Previous atomistic Kinetic Monte Carlo (KMC) calculations: addition of Re causes transition from 1D SIA diffusion to 3D W-Re mixed dumbbell diffusion
- Experiments in W-Re alloys: Increasing Re content caused transition from ordered GBS to disordered gas bubbles
- **Suggests 1D SIA diffusion is primary driver of GBS formation**

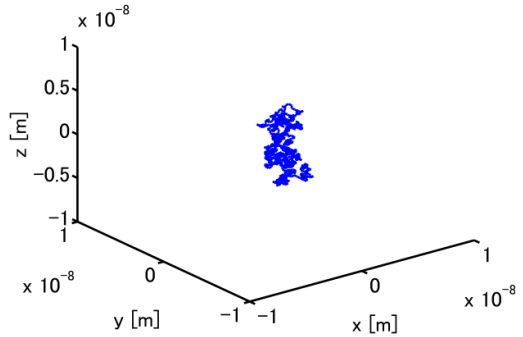

Path of <111> W-Re mixed dumbbell by KMC

Suzudo et al, JNM. 467, p. 418 (2015)

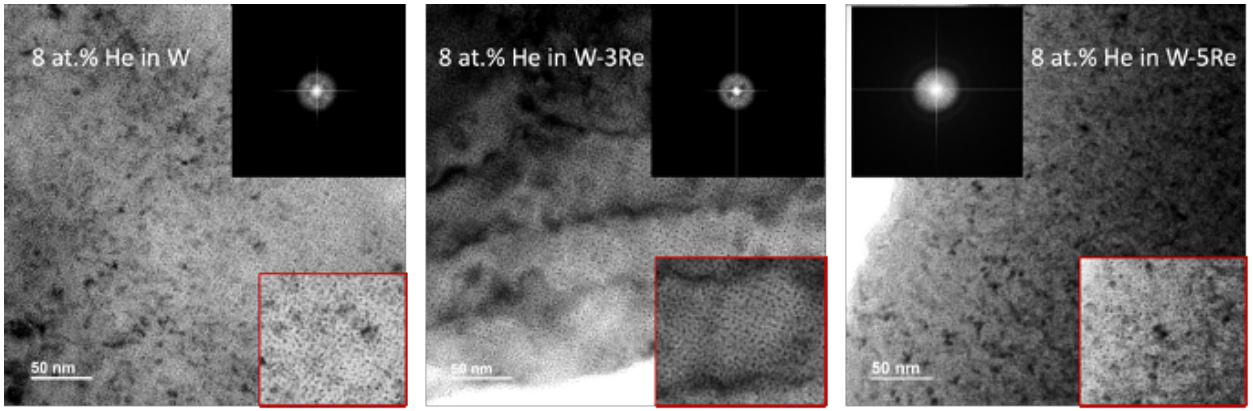

He at.%	2%	4%	6%	8%	10%	15%
W	Order	Order	Order	Order	Order	Order
W-3Re	Disorder	Disorder	Order	Order	Order	Order
W-5Re	Disorder	Disorder	Disorder	Disorder	Disorder	Disorder

Computational Microstructure Science Group

Thanks for your attention!

Funding Support: DOE-NE NEAMS Program

NEAMS
NUCLEAR ENERGY ADVANCED MODELING & SIMULATION PROGRAM

Questions?

Phase-field model initial conditions

- Determine $F_{c,sat}$
- 1035 K
- $\theta/2 = 73$
- No-flux boundary conditions
- 3 μm × 3 μm grain boundary
- Populate with randomly placed lenticular bubbles, n_a = 15 / μm^2, minimum spacing 160 nm

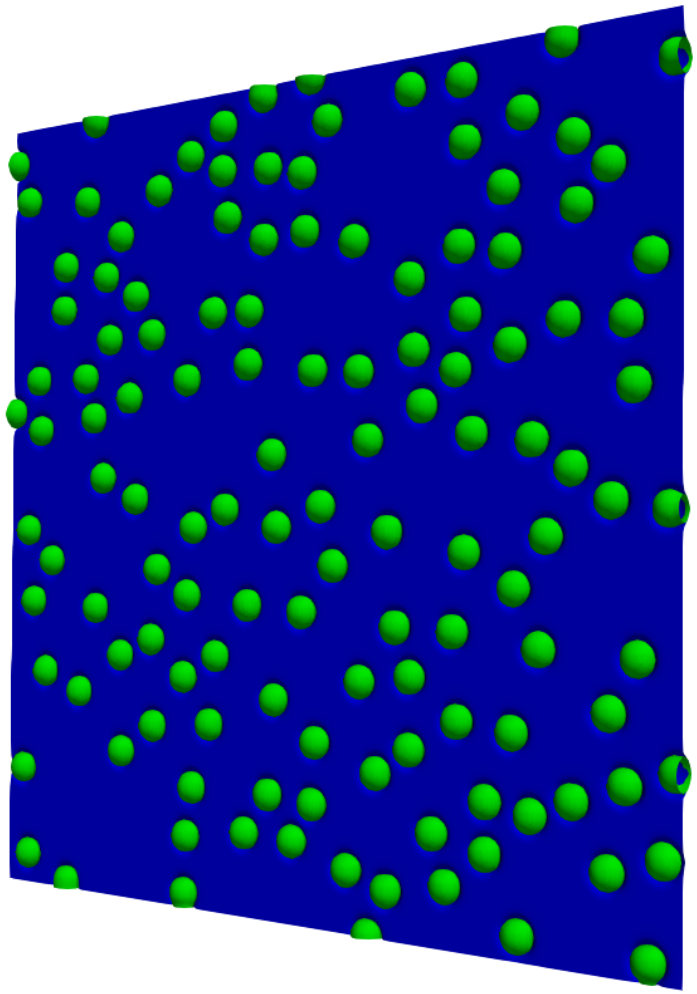

3 μm × 3 μm

Electrochemical grand potential densities

- Typically, phase-field models use Helmholtz free energy
  - Solid and void phases: and
- To take advantage of grand potential formulation, need to perform Legendre transform of each phase's Helmholtz free energy to obtain electrochemical grand potential densities of solid and void phases, and :

$$\omega_s = f_{ec,s} - \mu_{V_Y} n^s_{V_Y} - \mu_{V_O} n^s_{V_O} - \vec{D} \cdot \vec{E}$$

$$\omega_v = f_{ec,v} - \mu_{V_Y} n^v_{V_Y} - \mu_{V_O} n^v_{V_O} - \vec{D} \cdot \vec{E}$$

- , : chemical potentials
- Transforms independent variables to , ,

Electrochemical free energies of each phase

- Sum of chemical and electrostatic energy contributions: for solid,

$$f_{ec,s} = f_{chem,s} + f_{es,s}$$

- Chemical contribution: dilute solution or parabolic approximation

$$f^{d}_{chem,s} = n^{s}_{V_Y} E^{s}_{V_Y} + n_Y kT \left(c^{s}_{V_Y} \ln c^{s}_{V_Y} - c^{s}_{V_Y} \right) + n^{s}_{V_O} E^{s}_{V_O} + n_O kT \left(c^{s}_{V_O} \ln c^{s}_{V_O} - c^{s}_{V_O} \right)$$

- To account for vacancy segregation energy to GBs,

$$E^{s}_{V_Y} = \left(E^{f}_{V_Y} + A \left(E^{GB}_{V_Y} - E^{f}_{V_Y} \right) (1-\lambda)^2 \right) \qquad \lambda = \sum_{i=1}^{n} \eta_i^2$$

- Electrostatic contribution:

$$f_{es,s} = \rho V + \frac{1}{2} \vec{D} \cdot \vec{E} \qquad \rho = \sum_i Z_i e n_i \qquad \vec{D} = \epsilon_s \vec{E}$$